Spatiotemporal variations of the $\delta(O_2/N_2)$, CO_2 and δ(APO) in the troposphere over the Western North Pacific

Shigeyuki Ishidoya[1], Kazuhiro Tsuboi[2], Yosuke Niwa[3], Hidekazu Matsueda[2], Shohei Murayama[1], Kentaro Ishijima[2], and Kazuyuki Saito[4]

[1]National Institute of Advanced Industrial Science and Technology (AIST), Tsukuba 305-8569, Japan,
[2]Meteorological Research Institute, Tsukuba, Japan, Tsukuba305-0052, Japan,
[3]National Institute for Environmental Studies, Tsukuba 305-8506, Japan
[4]Japan Meteorological Agency, Tokyo, Japan, Tokyo 105-8431, Japan

Correspondence to: Shigeyuki Ishidoya (s-ishidoya@aist.go.jp)

Abstract. We analyzed air samples collected onboard a cargo aircraft C-130 over the western North Pacific from May 2012 to March 2020 for atmospheric $\delta(O_2/N_2)$ and CO_2 amount fraction. Observations were corrected for significant artificial fractionation of O_2 and N_2 caused by thermal diffusion during the air sample collection by using the simultaneously-measured $\delta(Ar/N_2)$. The observed seasonal cycles of the $\delta(O_2/N_2)$ and atmospheric potential oxygen (δ(APO)) varied nearly in opposite phase to that of the CO_2 amount fraction at all latitudes and altitudes. Seasonal amplitudes of δ(APO) decreased with latitude from 34 to 25° N, as well as with increasing altitude from the surface to 6 km by 50–70 %, while those of CO_2 amount fraction decreased by less than 20%. By comparing the observed values with the simulated δ(APO) and CO_2 amount fraction values generated by an atmospheric transport model, we found that the seasonal δ(APO) cycle in the middle troposphere was modified significantly by a combination of the northern and southern hemispheric seasonal cycles due to the inter-hemispheric mixing of air. The simulated δ(APO) underestimated the observed interannual variation in δ(APO) significantly, probably due to the interannual variation in the annual mean air-sea O_2 flux. Interannual variation in δ(APO) driven by the net marine biological activities, obtained by subtracting the assumed solubility-driven component of δ(APO) from the total variation, indicated a clear influence on annual sea-to-air (air-to-sea) marine biological O_2 flux during El Niño (La Niña). By analyzing the observed secular trends of $\delta(O_2/N_2)$ and CO_2 amount fraction, global average terrestrial biospheric and oceanic CO_2 uptakes for the period 2012–2019 were estimated to be (1.8 ± 0.9) and (2.8 ± 0.6) Pg a^{-1} (C equivalents), respectively.

1 Introduction

Atmospheric O_2/N_2 ratios have been observed since the early 1990s, for the primary application of constraining the marine and terrestrial exchange of CO_2 (Keeling and Shertz, 1992). For this purpose, observations of the O_2/N_2 ratio have been carried out at many surface stations and on commercial cargo ships (e.g., Bender et al., 2005; Manning and Keeling, 2006; Tohjima et al., 2008, 2019; Goto et al., 2017). The O_2/N_2 ratio varies in opposite phase with CO_2 amount fraction due to the

terrestrial biosphere exchanges and fossil fuel combustion, of which respective O_2:CO_2 exchange ratios (oxidative ratio (OR) = $-\Delta y(O_2)\Delta y(CO_2)^{-1}$ mol mol^{-1}) are about 1.1 and 1.4, respectively (Keeling, 1988; Severinghaus, 1995), where y stands for the dry amount fraction of gas, as recommended by the IUPAC Green Book (2007). By using the OR value of 1.1 for terrestrial biospheric activities, Atmospheric Potential Oxygen (APO) is defined by $y(APO) = y(O_2) + 1.1y(CO_2)$ (Stephens et al., 1998). While APO is conserved for terrestrial biospheric activities, the air-sea exchange of O_2 is much faster than that of CO_2 since the air-sea CO_2 exchange is highly suppressed by the carbonate buffer system in seawater (e.g. Keeling et al., 1993). Therefore, APO can be used to evaluate air-sea O_2 fluxes associated with marine biological and physical processes (e.g. Nevison et al., 2012).

Aircraft observation serves as a useful platform for measuring altitude-dependent APO driven by spatially-integrated air-sea O_2 fluxes at the surface. Aircraft observations of the O_2/N_2 ratio have been conducted in the past (e.g. Sturm et al., 2005; Steinbach, 2010; Ishidoya et al., 2008a, 2012, 2014; van der Laan et al., 2014; Bent, 2014; Morgan et al., 2019; Birner et al., 2020; Stephens et al., 2018, 2021). Sturm et al. (2005) observed a vertical gradient and seasonal cycle in the O_2/N_2 ratio in the height range of 0.8-3.1 km over Perthshire, United Kingdom, for the period 2003-2004. Longer term observations of the tropospheric O_2/N_2 ratio have also been carried out by Ishidoya et al. (2012) and van der Laan et al. (2014). They conducted aircraft observations at heights of 2, 4 and above 8 km over Japan during 1999-2010 and at heights of 0.1 and 3 km over western Russia during 1998-2008, respectively, and provided additional evidence of seasonal cycles and secular changes in the tropospheric O_2/N_2 ratio. However, there were uncertainties associated with artificial fractionations of O_2 and N_2 in Ishidoya et al. (2012) and van der Laan et al. (2014). Ar/N_2 ratio and/or stable isotopic ratios can be used to evaluate natural and artificial molecular-diffusive fractionations of O_2 and N_2 (e.g. Kawamura et al., 2006; Ishidoya et al., 2013), however Ishidoya et al. (2012) and van der Laan et al. (2014) did not observe them.

Ishidoya et al. (2014) and Stephens et al. (2021) observed O_2/N_2 and Ar/N_2 simultaneously, and were able to correct for thermally-diffusive artificial fractionation of O_2/N_2, by using coefficients of 3.54 and 3.77 of Ar/O_2, respectively. By using the corrected O_2/N_2 ratio, Ishidoya et al. (2014) were able to observe spatiotemporal variations in the O_2/N_2 ratio from the surface to the middle troposphere over the western North Pacific around Japan, on monthly scheduled flights, for the period May 2012 to April 2013. Similarly, Stephens et al. (2021) were able to provide a better picture of much wider-area distributions of O_2/N_2 ratio, from 0–14 km and 87° N to 85° S, using measurements from a series of aircraft campaigns such as five HIAPER Pole-to-Pole Observations campaigns (HIPPO) in 2009-2011 (Wofsy et al., 2011), and the O_2/N_2 Ratio and CO_2 Airborne Southern Ocean (ORCAS) study in 2016 (Stephens et al., 2018).

Stephens et al. (2021) also conducted continuous observations of O_2 mole fraction using a vacuum ultraviolet (VUV) absorption detector (Stephens et al., 2003). They adjusted the continuous O_2 data to the simultaneously observed flask-based O_2/N_2 ratio corrected for the artificial fractionation using Ar/N_2 ratio, since the artificial fractionations for the continuous observations were more significant than that for the flask sampling due to the lower flow rate. Based on the continuous O_2 data, Morgan et al. (2019) reported summertime vertical gradients of the atmospheric O_2/N_2 ratio and CO_2 amount fraction through the atmospheric boundary layer over the Drake Passage region of the Southern Ocean, to evaluate the air-sea O_2/CO_2

flux ratios in the region. Aircraft observations of Ar/N_2 are also used to evaluate gravitational separation of the atmospheric components, which is an indicator of the Brewer-Dobson circulation (e.g. Ishidoya et al., 2013), in the lowermost stratosphere under the condition that the artificial fractionation is reduced sufficiently (Ishidoya et al., 2008; Birner et al., 2020).

In this study, as an update to Ishidoya et al. (2014), we present 9-year-long O_2/N_2 ratio variations observed in the troposphere over the western North Pacific. Measurements were carried out on monthly scheduled cargo aircraft flights with a fixed flight route, and the thermally-diffusive artificial fractionations on O_2/N_2 ratio were corrected by using simultaneously-measured Ar/N_2 ratio. Using these corrected values, we made precise evaluation of the height-latitude distributions of seasonal cycle, vertical profile and year-to-year variation along the flight route. We mainly focus our discussions on the variations in the tropospheric APO and CO_2 amount fraction with the aid of a 3-D atmospheric chemistry-transport model. We also estimate average terrestrial biospheric and oceanic CO_2 uptakes for the period 2012–2019, by using long-term trends of O_2/N_2 ratio and CO_2 amount fraction.

2 Methods

The cargo aircraft C-130 flies once per month from Atsugi Base (35.45° N, 139.45° E), Kanagawa, Japan, to Minamitorishima, Japan, a small coral atoll (MNM; 24.29° N, 153.98° E). The cruising altitude is about 6 km, and 24 air samples were pressurized into 1.7 L silica-coated titanium flasks to an absolute pressure of 0.4 MPa during the flight. A set of 17–20 samples were collected during the level flight while others were collected during the descent portion at MNM. Flask air sampling for the C-130H flight is manually operated by two JMA personnel on board the aircraft. Therefore, a diaphragm pump is modified to be operated by hand, without the electric power supply. Air samples are collected from the air-conditioning system in the C-130H aircraft. Fresh air outside the aircraft is compressed by an engine and fed into the air-conditioning ducts by passing it through a pneumatic system and air cycle packs. A Teflon tube with a diameter of 1/4 in. for the air sampling intake is inserted into the air-conditioning bowing nozzle upstream of the recirculation fan so that the sample air is not contaminated with the cabin air. The open end of the air sampling intake is situated at wing root and faces the front side of the aircraft. It is noted that we use Teflon tube in the upstream of the diaphragm pump only to avoid absorption and/or permeation of O_2 due to a pressurization of the tube. In this regard, we found measured values of O_2/N_2 ratio for the air samples corrected in January, 2016 were anomalously low, when Teflon tube was used in the downstream of the diaphragm pump. Therefore, we exclude the O_2/N_2 ratio values in January 2016 from the analyses in this study. Details of the air sampling method has been described elsewhere (Tsuboi et al., 2013).

The flask air samples were brought back to the Japan Meteorological Agency (JMA) and analyzed for CO_2, CH_4, CO and N_2O amount fractions. The observational results are reported by Niwa et al. (2014). The CO_2 amount fraction was measured using a non-dispersive infrared analyzer (Licor, LI-7000) with a precision of better than ±0.07 ppm (Tsuboi et al., 2013) against the World Meteorological Organization (WMO) mole fraction scales for CO_2 (Zhao and Tans, 2006). The dataset is posted on the WMO's World Data Centre for Greenhouse Gases (WMO/WGCGG, http://ds.data.jma.go.jp/gmd/wdcgg/wdcgg.html).

After the JMA analyses, the flasks were sent to the National Institute of Advanced Industrial Science and Technology (AIST) to measure O_2/N_2 and Ar/N_2 ratios, as well as the stable isotopic ratios of N_2, O_2 and Ar (Ishidoya et al., 2014). In this study, we present the measured data obtained from the air samples collected for the period May 2012 – March 2020. In Fig. 1, we show all the locations where the air samples were collected onboard C-130 aircrafts during the observation period, and the locations of MNM, Atsugi Base and Ioto Island (24.76° N, 141.29° E), Japan.

The values of $\delta(O_2/N_2)$, $\delta(Ar/N_2)$, stable isotopic ratios of N_2, O_2 and Ar ($\delta(^{15}N)$, $\delta(^{18}O)$ and $\delta(^{40}Ar)$) are reported in per meg (one per meg is equal to 1×10^{-6}):

$$\delta(O_2/N_2) = \frac{R_{sample}(^{16}O^{16}O/^{14}N^{14}N) - R_{standard}(^{16}O^{16}O/^{14}N^{14}N)}{R_{standard}(^{16}O^{16}O/^{14}N^{14}N)}, \quad (1)$$

$$\delta(Ar/N_2) = \frac{R_{sample}(^{40}Ar/^{14}N^{14}N) - R_{standard}(^{40}Ar/^{14}N^{14}N)}{R_{standard}(^{40}Ar/^{14}N^{14}N)}, \quad (2)$$

$$\delta(^{15}N) = \frac{R_{sample}(^{15}N^{14}N/^{14}N^{14}N) - R_{standard}(^{15}N^{14}N/^{14}N^{14}N)}{R_{standard}(^{15}N^{14}N/^{14}N^{14}N)}, \quad (3)$$

$$\delta(^{18}O) = \frac{R_{sample}(^{18}O^{16}O/^{16}O^{16}O) - R_{standard}(^{18}O^{16}O/^{16}O^{16}O)}{R_{standard}(^{18}O^{16}O/^{16}O^{16}O)}, \quad (4)$$

$$\delta(^{40}Ar) = \frac{R_{sample}(^{40}Ar/^{36}Ar) - R_{standard}(^{40}Ar/^{36}Ar)}{R_{standard}(^{40}Ar/^{36}Ar)}, \quad (5)$$

where the subscripts 'sample' and 'standard' refer to the values of the sample and standard air, respectively. The values of $\delta(O_2/N_2)$, $\delta(Ar/N_2)$, $\delta(^{15}N)$, $\delta(^{18}O)$ and $\delta(^{40}Ar)$ of the air samples were determined against our primary standard air (cylinder No. CRC00045) by using a mass spectrometer (Thermo Scientific Delta-V) (Ishidoya and Murayama, 2014) with a respective reproducibility of about 5, 8, 1.5, 3 and 13 per meg (1σ). The scale based on the primary standard air is our original scale and called as "EMRI/AIST scale" in Aoki et al. (2021).

As already discussed in Ishidoya et al. (2014), the measured values of $\delta(O_2/N_2)$ are contaminated by significant artificial thermally-diffusive fractionation of O_2 and N_2 during the air sample collection process onboard the aircraft. Figure 2 shows the relationships between $\delta(Ar/N_2)$, $\delta(^{18}O)$ and $\delta(^{40}Ar)$ with $\delta(^{15}N)$ for all the air samples analyzed in this study. It was found that $\delta(Ar/N_2)$, $\delta(^{18}O)$ and $\delta(^{40}Ar)$ change linearly in proportion to $\delta(^{15}N)$, and the linear regression analyses gave respective slopes of (16.3 ± 0.1), (1.58 ± 0.01) and (2.69 ± 0.05) per meg per meg^{-1} for the $\delta(Ar/N_2)/\delta(^{15}N)$, $\delta(^{18}O)/\delta(^{15}N)$ and $\delta(^{40}Ar)/\delta(^{15}N)$ ratios. These ratios agree well with the ratios of (16.2 ± 0.1), (1.55 ± 0.02) and (2.75 ± 0.05) for $\delta(Ar/N_2)/\delta(^{15}N)$, $\delta(^{18}O)/\delta(^{15}N)$ and $\delta(^{40}Ar)/\delta(^{15}N)$, respectively, determined from the laboratory experiments on the effect of thermally-diffusive fractionations on $\delta(Ar/N_2)$, $\delta(^{15}N)$, $\delta(^{18}O)$ and $\delta(^{40}Ar)$ (Ishidoya et al., 2013). Therefore, we decided to correct for the thermally-diffusive fractionation of O_2 and N_2 on the observed $\delta(O_2/N_2)$ by using the following equation (Ishidoya et al., 2014):

$$\delta_{cor.}(O_2/N_2) = \delta_{meas.}(O_2/N_2) - \alpha_{O_2} \cdot \alpha_{Ar}{}^{-1} \cdot \Delta\delta_{meas.}(Ar/N_2), \quad (6)$$

Here, $\delta_{cor.}(O_2/N_2)$ and $\delta_{meas.}(O_2/N_2)$ denote the corrected and measured $\delta(O_2/N_2)$, respectively. The coefficients α_{O2} = (4.57 ± 0.02) and α_{Ar} = (16.2 ± 0.1) are the $\delta(O_2/N_2)/\delta(^{15}N)$ and $\delta(Ar/N_2)/\delta(^{15}N)$ ratios respectively, determined from the laboratory

experiments as described by Ishidoya et al. (2013). The value for α_{O2} is not directly reported in Ishidoya et a. (2013) but it was obtained from the same laboratory experiment (Fig. 2 in their study). The α_{O2}/α_{Ar} ratio of 4.57/16.2 is close to the Keeling et al. (2004) diffusion factor for $(Ar/N_2)/(O_2/N_2)$ and results in the same tracer $\delta(O_2/N_2)^*$ (Stephens et al., 2020). $\Delta\delta_{meas.}(Ar/N_2)$ is the deviation of the measured $\delta(Ar/N_2)$ from its reference point that is determined by using the annual mean value of $\delta(Ar/N_2)$ in 2013 observed at the surface in Tsukuba (36° N, 140° E), Japan (Ishidoya and Murayama, 2014). The effect of the seasonal $\delta(Ar/N_2)$ cycle on $\delta_{cor.}(O_2/N_2)$ was therefore not excluded in this study; this could lead to an over (under)-correction of the surface $\delta_{cor.}(O_2/N_2)$ by about 2 per meg in the summertime (wintertime). Considering the measurement reproducibility of $\delta_{meas.}(O_2/N_2)$ of 5 per meg, uncertainty of the correction of 2 per meg (8 per meg x $\alpha_{O2}\ \alpha_{Ar}^{-1}$; 8 per meg is the measurement reproducibility of $\delta_{meas.}(Ar/N_2)$) and the $\delta(Ar/N_2)$ seasonality, the overall uncertainty of $\delta_{cor.}(O_2/N_2)$ was evaluated to be less than 6 per meg. It is noted that the annual mean value of $\delta(Ar/N_2)$ also shows interannual variation with a peak-to-peak amplitude of 9 per meg a^{-1} and secular trend of 0.75 per meg a^{-1} (Ishidoya et al., 2021). They result in uncertainties of $\delta_{cor.}(O_2/N_2)$ by 2.5 and 0.1 per meg y^{r-1} for the interannual variation and secular trend, respectively, which are significantly smaller than those of the observed $\delta_{cor.}(O_2/N_2)$ discussed below. The details of the correction of artificial fractionations of O_2 and N_2 is given in Ishidoya et al. (2014). It is noted that the correction by using $\delta(^{15}N)$, which is stable in the atmosphere over long time period, is also suitable to obtain $\delta_{cor.}(O_2/N_2)$. Since the uncertainty of the corrected $\delta_{cor.}(O_2/N_2)$ by using $\delta(^{15}N)$ is ±7 per meg (±1.5 x 4.57), which is larger than that by using $\delta(Ar/N_2)$ (±2 per meg), we determined to use $\delta(Ar/N_2)$ rather than $\delta(^{15}N)$ in the present study.

We used δ(APO) for the detailed analyses of the air-sea exchange of O_2. δ(APO) was calculated from the observed $\delta_{cor.}(O_2/N_2)$ and CO_2 amount fraction in per meg;

$$\delta(\mathrm{APO}) = \delta_{\mathrm{cor.}}(\mathrm{O_2/N_2}) + \frac{\alpha_{\mathrm{B}}}{X_{\mathrm{O2}}} y(\mathrm{CO_2}) \times 10^6 - 2000, \quad (7)$$

where $y(CO_2)$ is the dry amount fraction of CO_2, α_B is the OR of 1.1 for terrestrial biospheric activities, X_{O2} of 0.2093 – 0.2094 is the amount fraction of atmospheric O_2 (Tohjima et al., 2005; Aoki et al., 2019), and 2000 is an arbitrary reference. From the definition, δ(APO) is conserved for terrestrial biospheric activities, and driven by not only air-sea exchange of O_2, N_2 and CO_2 but also fossil fuel consumption of which OR value is generally larger than 1.1 (Keeling, 1988). In order to investigate the observed $\delta_{cor.}(O_2/N_2)$ variations, we used a three-dimensional atmospheric transport model NICAM-TM (Niwa et al., 2011) to simulate CO_2 amount fraction and δ(APO) using surface O_2, N_2 and CO_2 fluxes. NICAM-TM is based on the Nonhydrostatic ICosahedral Atmospheric Model (NICAM: Satoh et al., 2008, 2014) and its tracer transport version has been used for atmospheric transport and flux inversion studies of greenhouse gases (e.g. Niwa et al. 2012). The horizontal model resolution used in this study had a mean grid interval of about 112 km. The model was driven by nudging the horizontal winds towards the Japanese 55-year Reanalysis data (JRA-55: Kobayashi et al., 2015).

The surface fluxes incorporated into NICAM-TM were the air-sea fluxes of O_2, N_2 and CO_2, and also CO_2 and O_2 fluxes from fossil fuel combustion. The air-sea O_2 and N_2 fluxes were the climatological seasonal anomalies taken from the TransCom

experimental protocol (Blain, 2005; Garcia and Keeling 2001). The fluxes were computed to give the seasonal component and the annual mean values at every grid point to be zero. The air-sea CO_2 flux was obtained from the monthly sea surface CO_2 flux climatology of Takahashi et al. (2009). The CDIAC fossil fuel database was used for the fossil fuel CO_2 flux (Andres et al., 2016; Gilfillan et al., 2019). Model-based δ(APO), CO_2 amount fraction and $\delta(O_2/N_2)$ were calculated using the following equations (e.g. Tohjima et al., 2012) in per meg, ppm and per meg, respectively:

$$\delta(\mathrm{APO}) = \left(\frac{y^{\mathrm{SA}}(\mathrm{O_2})}{X_{\mathrm{O2}}} - \frac{y^{\mathrm{SA}}(\mathrm{N_2})}{X_{\mathrm{N2}}}\right) + \left(\frac{-\alpha_{\mathrm{F}} \cdot y^{\mathrm{FF}}(CO_2) + \alpha_{\mathrm{B}} \cdot y^{\mathrm{FF}}(CO_2)}{X_{\mathrm{O2}}}\right) + \frac{\alpha_{\mathrm{B}} \cdot y^{\mathrm{OC}}(CO_2)}{X_{\mathrm{O2}}}, \quad (8)$$

$$y(\mathrm{CO_2}) = y^{\mathrm{FF}}(\mathrm{CO_2}) + y^{\mathrm{OC}}(\mathrm{CO_2}) + y^{\mathrm{TB}}(\mathrm{CO_2}), \quad (9)$$

$$\delta(\mathrm{O_2/N_2}) = \left(\frac{y^{\mathrm{SA}}(\mathrm{O_2})}{X_{\mathrm{O2}}} - \frac{y^{\mathrm{SA}}(\mathrm{N_2})}{X_{\mathrm{N2}}}\right) + \frac{-\alpha_{\mathrm{F}} \cdot y^{\mathrm{FF}}(CO_2)}{X_{\mathrm{O2}}} + \frac{-\alpha_{\mathrm{F}} \cdot y^{\mathrm{TB}}(CO_2)}{X_{\mathrm{O2}}}, \quad (10)$$

where $y(O_2)$, $y(N_2)$ and $y(CO_2)$ are dry amount fractions of the respective gases calculated using NICAM-TM. The superscripts "SA", "FF", "OC" and "TB" denote the seasonal anomaly of the air-seas O_2 and N_2 flux, CO_2 flux from fossil fuel combustion, ocean and terrestrial biosphere, respectively. X_{O2} and α_B have the same meaning as in Equation (7), while X_{N2} is the dry amount fraction of N_2 in the atmosphere and α_F is the global average OR for fossil fuel combustion. In this study, we adopted X_{N2} = 0.7808 and α_F = 1.37. The α_F was calculated from the fossil fuel and cement production emissions by fuel type for the period 2012-2019, reported by GCP (Friedlingstein et al., 2020), and the oxidative ratios for the different fuel type were taken from Keeling (1988). It should be noted that $\delta_{cor.}(O_2/N_2)$, CO_2 amount fraction and δ(APO) obtained from NICAM-TM are reported as deviations from arbitrary reference points, in other words, reported on different scales from those of observations. We can rewrite equation (8) as:

$$\delta(\mathrm{APO}) = \delta^{\mathrm{SA}}(\mathrm{APO}) + \delta^{\mathrm{FF}}(\mathrm{APO}) + \delta^{\mathrm{OC}}(\mathrm{APO}). \quad (11)$$

The δ(APO) simulation run incorporating the above-mentioned surface fluxes is referred to as the "control run". In this calculation, δ(APO) driven by an annual mean air-sea O_2 and N_2 fluxes (hereafter referred to as the "δ^{AM}(APO)"), which were estimated by Gruber et al. (2001), was ignored. In other words, the δ(APO) obtained from the NICAM-TM control run ignore the contribution of not only interannual variations but also spatial distribution in annual mean air-sea O_2 and N_2 fluxes. If the control run represents other components other than δ^{AM}(APO) correctly, then the contribution of δ^{AM}(APO) was evaluated by subtracting the simulated δ(APO) from the observed δ(APO). In Sections 3-2, we will discuss interannual variation in this context.

3 Results and discussion

3.1 Latitudinal and vertical distributions of $\delta_{cor.}(O_2/N_2)$, CO_2 amount fraction and δ(APO)

Figure 3(a) shows the measured $\delta(O_2/N_2)$ and $\delta(Ar/N_2)$ for all the air samples observed in this study, and Fig. 3(b) shows the $\delta_{cor.}(O_2/N_2)$ corrected values by applying eq. (6) to the measured values. As seen from the figures, significant artificial fractionations found in the measured $\delta(O_2/N_2)$ are reduced dramatically by the correction. It can also be seen from Fig. 3(a)

that the fractionations have become smaller since 2018, especially at the higher altitude. It should be noted that these noted changes across 2018 could be at least partly related to changes in the aircraft type from C-130H to C-130R used for flask sampling. The periods when the C-130R were used are indicated by pale red shade. No systematic data gaps were found in the $\delta_{cor.}(O_2/N_2)$ time series across 2018, so that we successfully corrected the fractionation of O_2 and N_2 both for C-130H and C-130R. To examine the validity of the significant corrections applied to the $\delta_{meas.}(O_2/N_2)$, we also show the vertical profiles of detrended $\delta_{cor.}(O_2/N_2)$ separated by season in Fig. 3(c), obtained by subtracting a linear secular trend from the data in Fig. 3(b). As seen from the figure, seasonal $\delta_{cor.}(O_2/N_2)$ variations with summertime maxima are clearly seen at all altitudes, which supports validity of the correction. We also presented some examples that synoptic-scale variations in $\delta(O_2/N_2)$ can also be reproduced by using $\delta_{cor.}(O_2/N_2)$ in our previous study (Fig. 4 in Ishidoya et al. (2014)).

Figure 4(a) shows variations in the $\delta_{cor.}(O_2/N_2)$, CO_2 amount fraction and δ(APO) observed in the layer (6.1 ± 0.5) km (±1σ) (hereafter referred to as "middle troposphere") at five latitudes over the western North Pacific. Best-fitted curves to the data and secular trends obtained using a digital filtering technique (Nakazawa et al., 1997a) are also shown. In the filtering technique, the average seasonal cycles were approximated by fundamental and its first harmonics, and signals with periods longer than 36 months were regarded as contributing to a secular trend. The observational data deviated from the best-fitted curves more than ±3σ are excluded from the analyses and not shown in the figures discussed in this study (2% of the observational data are excluded in total). As can be seen in Fig. 4(a), secular decreases in $\delta_{cor.}(O_2/N_2)$ and δ(APO) and increases in CO_2 amount fraction, accompanied by prominent seasonal cycles, were observed at each latitude. The secular changes in $\delta_{cor.}(O_2/N_2)$ and CO_2 amount fraction can be attributed mainly to O_2 consumption and CO_2 emission resulting from fossil fuel combustion. The seasonally dependent air-sea O_2 flux and the terrestrial biospheric activity contribute towards the observed seasonal $\delta(O_2/N_2)$ cycle, while the terrestrial biospheric activity is the main contributor to the seasonal CO_2 amount fraction cycle (e.g. Keeling et al., 1993; Keeling and Manning, 2014). The average rates of change in the observed $\delta_{cor.}(O_2/N_2)$, CO_2 amount fraction and δ(APO) at the four latitudes shown in Fig. 4(a) were (-24.2 ± 0.4) per meg a^{-1}, (2.43 ± 0.05) ppm a^{-1} and (-11.3 ± 0.4) per meg a^{-1}, respectively, for the observational period. General features of the observed variations in $\delta(O_2/N_2)$, CO_2 amount fraction and δ(APO) are well reproduced by the control run of NICAM-TM, as shown in Fig. 4(b). Figure 5(a) shows variations in $\delta_{cor.}(O_2/N_2)$, CO_2 amount fraction and δ(APO) observed over MNM. Clear secular trends and prominent seasonal cycles of $\delta_{cor.}(O_2/N_2)$, CO_2 amount fraction and δ(APO) are distinguishable, similar to those in Fig. 4(a). We also note in Fig. 5(a) that the seasonal amplitudes of $\delta_{cor.}(O_2/N_2)$, CO_2 amount fraction and δ(APO) decrease with increasing altitudes. These features are also reproduced by the control run of NICAM-TM (Fig. 5(b)).

Figure 6(a) shows average seasonal cycles of δ(APO) and CO_2 amount fraction observed at five latitudes over the western North Pacific. They show clear seasonal cycles with summertime maxima in δ(APO) and minima in CO_2. However, the amplitude of seasonal δ(APO) cycle decreases significantly toward the lower latitudes, with seasonal maxima and minima clearly occurring earlier than those of the CO_2 cycle. Figure 6(b) shows the corresponding average seasonal cycles of δ(APO)

and CO_2 amount fraction obtained from the control run of NICAM-TM. Earlier appearances of the seasonal maxima and minima in δ(APO) than those in CO_2 amount fraction are reproduced by NICAM-TM. The seasonal amplitude of the simulated δ(APO) also decreases toward the lower latitudes, in agreement with the observation, but is underestimated. As for the CO_2 amount fraction, the simulated seasonal cycles agree well with the observations. In Figs. 6(c) and (d), we also show same average seasonal cycles of the observed and simulated δ(APO) in Figs. 6(a) and (b), respectively, along with the detrended observed values at each latitude for the convenience of visual comparison between the observed and simulated results.

Figure 7(a) shows average seasonal cycles of δ(APO) and CO_2 amount fraction observed over MNM. The δ(APO) seasonal cycle varies in opposite phase from the CO_2 amount fraction. However, amplitudes of the seasonal δ(APO) cycle decrease significantly with the higher altitude, with seasonal minima clearly occurring earlier than those of the CO_2 cycle. These salient characteristics are reproduced generally by the NICAM-TM control run (Fig. 7(b)). Similar to Fig. 6, we also show Figs. 7(c) and (d) for visual comparison between the observed and simulated results.

In order to identify and explore some of the cause(s) that gave rise to the observed differences in the latitudinal/altitudinal changes in the seasonal cycles between δ(APO) and CO_2 amount fraction shown in Fig. 6(a) and 7(a), we carried out additional NICAM-TM simulations. In the calculation, we used the same fluxes that were used in the control run but for the northern hemispheric flux only for the TransCom seasonal climatology (hereafter referred to as "w/o SH flux run"). It is well known that the opposing phase of the seasonal δ(APO) cycles between the northern and southern hemispheres is due to seasonal changes in the air-sea O_2 (N_2) flux with summertime maxima (e.g. Keeling et al., 1998; Tohjima et al., 2012). Therefore, in comparing the control run with the w/o SH flux run, we decided to evaluate changes in the seasonal δ(APO) cycle by superimposing the anti-phase seasonal cycles through the inter-hemispheric mixing of air. On the other hand, seasonal CO_2 amount fraction cycle is much smaller in the southern hemisphere than that in the northern hemisphere (e.g. Nakazawa et al., 1997b). Therefore, it is expected that the seasonal cycle in CO_2 amount fraction in the northern hemisphere does not change significantly by the inter-hemispheric atmospheric mixing.

The seasonal δ(APO) cycles obtained from the w/o SH flux run are also shown in Figs. 6(b) and 7(b). As seen from Fig. 6(b), latitudinal differences in the seasonal δ(APO) amplitudes from the w/o SH flux run are clearly smaller than those from the control run. In addition, appearances of the maxima and minima of the seasonal δ(APO) cycle from the w/o SH flux run are later than those from the control run, pushing the timing closer to those of seasonal CO_2 amount fraction cycles. The seasonal δ(APO) cycles from the w/o SH flux run in Fig. 7(b) also show similar features. These results suggest that the inter-hemispheric mixing of air modifies the seasonal δ(APO) cycles significantly, especially in the higher altitude in the lower latitude region. To compare, in more detail, the observed latitudinal/altitudinal variation in the seasonal δ(APO) cycle amplitude with those calculated by NICAM-TM, Fig. 8(a) shows a latitudinal distribution of average fractions of the observed seasonal δ(APO) and CO_2 amount fraction amplitudes relative to the 33.5° N values. The decrease in the seasonal amplitude of δ(APO) toward the lower latitude is about 50%, while that of CO_2 amount fraction is less than 10%; these are well reproduced by the control run of NICAM-TM. On the other hand, the w/o SH flux run yields a decrease in the δ(APO)

amplitude by 20% toward the lower latitude, which is significantly smaller than that from the δ(APO) from control run, but slightly larger than that of CO_2 amount fraction. These results indicate that the SH makes a significant contribution to the amplitude and phase of the seasonal δ(APO) cycle at lower latitude.

Figure 8(b) shows average fractions of the seasonal amplitudes of δ(APO) and CO_2 amount fraction with height, relative to surface values. The surface seasonal cycles are obtained from continuous observations of $\delta(O_2/N_2)$ and CO_2 amount fraction at MNM since December 2015 (updated from Ishidoya et al., 2017). The seasonal amplitude of δ(APO) decreases rapidly with height by about 70%, while that of CO_2 amount fraction decreases by less than 20%. The altitudinal dependence of the seasonal δ(APO) amplitude is not consistent with that of CO_2. This could be attributed to the fact that the seasonal CO_2 cycle is driven mainly by terrestrial biospheric activities in the northern mid- and high latitudes and the seasonal minimum appears in summer, which makes the seasonal CO_2 cycle uniform from the surface to the middle troposphere due to continental strong convection in summer. On the other hand, seasonal APO cycle is driven by air-sea flux, so that altitudinal homogenization of the seasonal APO cycle due to convection is weaker than that of CO_2. These features are well reproduced by the control run of NICAM-TM. The altitudinal decrease in the seasonal δ(APO) amplitude is also reproduced by the w/o SH flux run, although a slight underestimation is found above 5 km. Therefore, the altitudinal decrease in the seasonal δ(APO) amplitude over MNM is mainly due to an attenuation of the seasonal air-sea O_2 and N_2 fluxes around MNM with height, with some influence from the inter-hemispheric atmospheric mixing. Consequently, over the western North Pacific region, the height-latitude distribution of seasonal δ(APO) cycles is more sensitive to the atmospheric transport processes associated with inter-hemispheric air mixing and vertical attenuation of surface signal, compared with those of seasonal CO_2 amount fraction cycles.

We also compared the observed and simulated annual mean values of δ(APO) and CO_2 amount fraction. Figure 9(a) shows average deviations of the middle tropospheric annual mean values of δ(APO) and CO_2 amount fraction at each latitude, relative to the 25.5° N values. The deviation values of δ(APO) and CO_2 amount fraction are well reproduced by the control and w/o SH flux runs. Therefore, the surface fluxes of O_2, N_2 and CO_2 in the northern hemisphere are the main contributors to the observed latitudinal variations in Fig. 9(a). As discussed in connection with eq. (11), we ignored δ^{AM}(APO) in our δ(APO) simulation using NICAM-TM, which is a component of δ(APO) driven by annual mean air-sea O_2 and N_2 fluxes. Therefore, the results of our simulation suggest that δ^{AM}(APO) does not affect significantly the latitudinal variations in the annual mean values of the middle tropospheric δ(APO) at 25-34° N. Figure 9(b) shows the height deviations of the annual mean values of δ(APO) and CO_2 amount fraction, relative to their corresponding values at 6 km over MNM. The observed profile of CO_2 amount fraction is well reproduced by NICAMT-TM. On the other hand, the average vertical gradient of δ(APO) profiles, obtained from the control and w/o SH flux runs of NICAM-TM, seems to be slightly larger than the observation. This may be due to the ignored contribution of δ^{AM}(APO); in that case, it may be that the sea area around MNM emits O_2 to the atmosphere throughout the observation period. Moreover, it is clearly seen from the figure that the interannual variation in the observed

δ(APO) profiles is much larger than that in the NICAM-TM simulations. This may also be due to the ignored contribution of δ^{AM}(APO), and we discuss interannual variations in the observed and simulated δ(APO) in the section below.

3.2 Interannual variations in δ(APO) and its implication to global air-sea O_2 flux and CO_2 budget

In this section, we discuss causes of the interannual variations found in the middle tropospheric δ(APO) observed over the western North Pacific. Figure 10(a) shows same secular trends in Fig. 4(a) and their annual change rates along with the deseasonalised values of δ(APO) at each latitude. The change rates observed at 29-34° N show interannual variation with maxima around the early 2015 and mid 2019, with a minimum at all latitudes in the early 2017. The corresponding change rates obtained from the control run of NICAM-TM are also shown in Fig. 10(b). The change rates obtained from NICAM-TM at 29-34° N show interannual variations in phase with the observed rates, although the amplitudes are smaller by about 80%. The interannual variations observed at 24-28° N are also larger than the simulated values. Therefore, it is likely that interannual variation in the δ^{AM}(APO), which was not incorporated into NICAM-TM, is a main contributor to the observed interannual variations at various latitudes. In this connection, it is possible that the interannual variation in the global air-sea CO_2 flux could also contribute to the larger interannual variation in the observed δ(APO) since the NICAM-TM model incorporated only the monthly sea surface CO_2 flux climatology to calculate δ^{OC}(APO). However, the global air-sea CO_2 flux reported by the Global Carbon Project (GCP) (Friedlingstein et al., 2020) showed an interannual variation of 0.07 Pg a^{-1} during 2012-2019, corresponding to 0.2 per meg a^{-1} of δ^{OC}(APO), which is much smaller than the interannual variation in the observed δ(APO) shown in Fig. 10.

By assuming that all other components besides δ^{AM}(APO) are well represented in the NICAM-TM control run, we subtracted the change rates simulated by NICAM-TM from the observed rates, to extract the interannual variations due only to the δ^{AM}(APO). The calculated change rates of δ^{AM}(APO) are shown at the bottom of Fig. 10(b). The change rates show similar interannual variations to the observed rates, but the latitudinal differences are smaller. This suggests that the interannual variations driven by δ^{AM}(APO) do not differ significantly as a function of latitude. In the following discussion, we make a bold assumption that an average of the change rates of δ^{AM}(APO) shown in Fig. 10(b) is a global average.

An anomaly of the average interannual variation of δ^{AM}(APO) change rate is shown in Fig. 11 (black line). In this figure, we also plotted a similar anomaly of interannual variation of the δ(APO) change rate due to solubility change (red line, hereafter referred to as "δ_{therm}(APO)"). The δ_{therm}(APO) was calculated from the δ(Ar/N_2) measurements observed at Tsukuba (36° N, 140° E), Japan (Ishidoya et al., 2021), by multiplying a coefficient of 0.84 derived from differences in the solubility in O_2 and Ar (Weiss 1970; Blaine, 2005). It should be noted that this is a rough approximation of the δ_{therm}(APO), which is a combination of air-sea fluxes of O_2, N_2, and CO_2 caused by solubility changes. As discussed in Ishidoya et al. (2021), the interannual variation in the δ(Ar/N_2) change rate is in phase with the global ocean heat content reported by ocean temperature measurements (e.g. Levitus et al., 2012). This suggests that δ_{therm}(APO) is also driven by changes in the solubility of the global

seawater. By subtracting δ_{therm}(APO) from δ^{AM}(APO), we estimated interannual variation of the δ(APO) change rate due to marine biological activities (green line, hereafter referred to as "δ_{netbio}(APO)"). It is expected that δ_{netbio}(APO) is driven by marine biological activities, not only in the surface mixed layer but also through a ventilation of subsurface low-O_2 waters.

Both the δ_{therm}(APO) and δ_{netbio}(APO) show significant interannual variations, roughly in opposite phase with each other. Moreover, the change rate of δ_{netbio}(APO) varies in opposite phase with the NINO.WEST (Japan Meteorological Agency, https://www.data.jma.go.jp/gmd/cpd/db/elnino/index/ninowidx.html), which is an index of El Niño-Southern Oscillation (ENSO). The ENSO is in the El Niño and La Niña phase, respectively, during the period with the negative and positive NINO.WEST index. Therefore, the δ_{netbio}(APO) tends to increase and decrease during El Niño and La Niña, respectively. This is consistent with Eddebber et al. (2017) who examined global and tropical air-sea O_2 flux responses to ENSO, based on the Community Earth System Model (CESM). They reported that the upper ocean loses O_2 to the atmosphere during El Niño and gains O_2 during La Niña mainly due to changes in ventilation of low-O_2 waters in the tropical Pacific, the region that has a dominant influence over the interannual variation in global air-sea O_2 flux (McKinley et al., 2003). By assuming the interannual variation in the δ_{netbio}(APO) represents a global average, and assuming a 1-box atmosphere with 5.124 x 10^{21} g for the total mass of dry air (Trenberth, 1981), 28.97 g mol^{-1} for the mean molecular weight of dry air, and respective fractions of 0.2093 and 0.7808 for O_2 and N_2 in the atmosphere, we estimated an interannual variation in the global air-sea O_2 flux due to marine biological activities (right axis of the green line in Fig. 11). The peak-to-peak amplitude of the O_2 flux is found to be about 300 Tmol yr^{-1}, which is almost consistent with that of global APO flux estimated using the δ(APO) data from Scripps stations (Keeling and Manning, 2014) and a global atmospheric transport inversion (Rödenbeck et al., 2008; Eddebber et al., 2017). Therefore, the seasonal cycles and interannual variations obtained from $\delta_{\mathrm{cor.}}(O_2/N_2)$ have a coherent signal we can explain, although we recognize the number of simplifying assumptions is extensive to derive δ_{netbio}(APO) and the aircraft observations are from a comparatively small region. This helps to prove that the$\delta_{\mathrm{cor.}}(O_2/N_2)$ are of good quality, even though the significant correction for enormous sampling artifacts.

By assuming the average secular trends of the middle tropospheric $\delta_{\mathrm{cor.}}(O_2/N_2)$ and CO_2 amount fraction observed in this study to be global average values, we were able to estimate the global CO_2 budget. The equations for separating out the global net terrestrial biospheric and oceanic CO_2 uptake are given by Keeling and Shretz (1992) firstly as;

$$B = \frac{\alpha_{\mathrm{F}}}{\alpha_{\mathrm{B}}} F + \frac{1}{0.471} \frac{X_{\mathrm{O2}}}{\alpha_{\mathrm{B}}} \frac{\mathrm{d}\delta(\mathrm{O_2/N_2})}{\mathrm{dt}} - \frac{Z_{\mathrm{eff}}}{\alpha_{\mathrm{B}}}, \quad (12)$$

and

$$O = -\frac{1}{0.471} \frac{\mathrm{d}}{\mathrm{dt}} \left(y(\mathrm{CO_2}) + \frac{X_{\mathrm{O2}}}{\alpha_{\mathrm{B}}} \delta(\mathrm{O_2/N_2}) \right) + \frac{\alpha_{\mathrm{B}} - \alpha_{\mathrm{F}}}{\alpha_{\mathrm{B}}} F + \frac{Z_{\mathrm{eff}}}{\alpha_{\mathrm{B}}}. \quad (13)$$

Here, B, F and O (in Pg yr^{-1}, C equivalents) are the global terrestrial biospheric CO_2 uptake, the anthropogenic CO_2 emitted from fossil fuel combustion and cement manufacturing, and the oceanic CO_2 exchange, respectively; $\mathrm{d}\delta(O_2/N_2)\mathrm{dt}^{-1}$ (per meg a^{-1}) and $\mathrm{d}y(CO_2)\mathrm{dt}^{-1}$ (ppm a^{-1}) are the observed change rates in atmospheric $\delta_{\mathrm{cor.}}(O_2/N_2)$ and CO_2 amount fraction, respectively;

0.471 converts CO_2 emissions of 1 Pg (C equivalents) to ppm of atmospheric CO_2; X_{O_2} is the standard mole fraction of O_2 in air (0.2093), α_F and α_B are the OR for global average fossil fuel combustion and net terrestrial biospheric activities, respectively; and Z_{eff} (Pg yr^{-1}) represents the net effect of oceanic O_2 outgassing on the oceanic and terrestrial biospheric CO_2 uptakes, which has been considered since Bender et al. (2005) and Manning and Keeling (2006). As described in Method section, we use α_F of 1.37 calculated from the fossil fuel and cement production emissions by fuel type reported by GCP.

Long-term change in Z_{eff} is caused mainly by stratification of the ocean and the decrease of O_2 solubility in seawater due to a secular increase in the global ocean heat content (e.g., Bopp et al., 2002). However, as discussed above for Fig. 11, the ocean O_2 outgassing shows significant interannual variation, which makes it difficult to estimate year-to-year variations in the global CO_2 budget from eqs. (12) and (13). In this regard, Tohjima et al. (2019) estimated the terrestrial biospheric and the oceanic CO_2 uptakes using their $\delta(O_2/N_2)$ and CO_2 amount fraction data, by changing the time period to obtain average secular change rates. They reported that the CO_2 uptakes estimated by using the change rates averaged over a longer period greater than 5 years were consistent with those reported by GCP (Le Quéré et al., 2018) within ±0.5 Pg a^{-1}, while those estimated using annual change rates scattered significantly.

It seems that the averaging period needed to reduce the interannual variations in δ_{therm}(APO) and δ_{netbio}(APO) in Fig. 11, is about 4-5 years, similar to Nevison et al. (2008) and Tohjima et al. (2019). Therefore, we estimated average terrestrial biospheric and oceanic CO_2 uptake throughout the observation period (2012-2019; 8-year) to reduce the interannual variation in Z_{eff} sufficiently. By using the global ocean (0-2000 m) heat content data from the National Oceanographic Data Center (NOAA)/National Centers for Environmental Information (NCEI) (updated from Levitus et al. 2012, https://www.nodc.noaa.gov/OC5/3M_HEAT_CONTENT/) and the same ratio of air-sea O_2 (N_2) flux to air-sea heat flux used in Manning and Keeling (2006), we adopted (0.6 ± 0.6) Pg a^{-1} for Z_{eff} for the period 2012-2019. We assumed 100% uncertainty for Z_{eff} following Manning and Keeling (2006). The value of F, (9.7 ± 0.5) Pg a^{-1}, was obtained from emissions from fossil fuel combustion and industrial processes by GCP (Friedlingstein et al., 2020). By using the average secular trends of $\delta_{cor.}(O_2/N_2)$ and CO_2 amount fraction for the observational period of the present study, the respective terrestrial biospheric and oceanic CO_2 uptakes were estimated to be (1.8 ± 0.9) and (2.8 ± 0.6) Pg a^{-1} for the period 2012-2019. These values agree well with the corresponding CO_2 uptake of (1.8 ± 1.1) and (2.6 ± 0.5) Pg a^{-1} reported by the GCP (Friedlingstein et al. 2020). It is noted that the terrestrial biospheric CO_2 uptake by GCP is calculated by subtracting the CO_2 emission due to land-use change ((1.6 ± 0.7) Pg a^{-1}) from their estimated total land CO_2 uptake ((3.4 ± 0.9) Pg a^{-1}).

4 Summary

Regular air samples were taken on cargo aircraft C-130 flights from Atsugi Base to MNM, and air samples have been collected during the level flight and during the descent portion at MNM. In this paper, we have presented the analytical results of the air samples for CO_2 amount fraction, $\delta(O_2/N_2)$, $\delta(Ar/N_2)$, $\delta(^{15}N)$ of N_2, $\delta(^{18}O)$ of O_2 and $\delta(^{40}Ar)$ for the period May 2012 – March

2020. The relationships of $\delta(Ar/N_2)$, $\delta(^{18}O)$ and $\delta(^{40}Ar)$ with $\delta(^{15}N)$ indicate a significant artificial fractionation due to thermal diffusion during the air sample collection.

The $\delta_{cor.}(O_2/N_2)$ values, corrected for the artificial fractionation by using $\delta(Ar/N_2)$, and the δ(APO) values derived from $\delta_{cor.}(O_2/N_2)$ were shown to have clear seasonal cycles nearly in opposite phase to that of the CO_2 amount fraction from the surface to 6 km along the latitudinal path from 25.5 to 33.5° N. We then used a three-dimensional atmospheric transport model NICAM-TM that was driven by the air-sea fluxes of O_2, N_2 and CO_2, along with fluxes of CO_2 and O_2 from fossil fuel combustion, to interpret some of the characteristic features we observed in the seasonal cycles and vertical profiles of APO and CO_2 amount fraction.

Seasonal amplitudes of δ(APO) and CO_2 amount fraction decreased toward the lower latitude from 34.5 to 24.5° N by about 50% and less than 10%, respectively: these features were reproduced by the corresponding ratios from the control run of NICAM-TM. On the other hand, the w/o SH flux run underestimated the latitudinal change in the δ(APO) amplitude, which indicated that the seasonal cycle of the mid-tropospheric δ(APO) was modified significantly by a combination of the northern and southern hemispheric seasonal cycles through the inter-hemispheric atmospheric mixing. The decrease in the δ(APO) seasonal amplitude was about 70% with height from the surface to 6 km, while that of CO_2 amount fraction was less than 20%. These features were also reproduced well by the control run of NICAM-TM.

The observed decrease in the annual mean values of CO_2 amount fraction with height was reproduced by the control run of NICAMT-TM. On the other hand, the average vertical gradient of the δ(APO) profiles was slightly overestimated by the NICAMT-TM simulations, while the simulated interannual variation was underestimated. This may be due to the ignored contribution of δ^{AM}(APO), which is a component of δ(APO) driven by annual mean air-sea O_2 and N_2 fluxes.

The interannual variations in the middle tropospheric δ^{AM}(APO) were estimated by subtracting the simulated δ(APO) by the NICAMT-TM control run from the observed δ(APO). We also estimated the solubility-driven component of δ(APO) (δ_{therm}(APO)) from the $\delta(Ar/N_2)$ observed at Tsukuba, assuming its interannual variation was driven by changes in the globally-averaged solubility of the seawater. The interannual variation in δ(APO) driven by marine biological activities (δ_{netbio}(APO)) was calculated by subtracting δ_{therm}(APO) from δ^{AM}(APO). The δ_{netbio}(APO) showed significant interannual variations in the opposite phase to that of δ_{therm}(APO), and the change rate varied in opposite phase with the NINO.WEST. Therefore, the δ_{netbio}(APO) values obtained in this study tended to increase and decrease with El Niño and La Niña, respectively, and is in agreement with Eddebber et al. (2017) who examined responses of the global and tropical air-sea O_2 flux to ENSO based on CESM.

By assuming the observed secular trends of the middle tropospheric $\delta_{cor.}(O_2/N_2)$ and CO_2 amount fraction to be representative of global average values, we estimated terrestrial biospheric and oceanic CO_2 uptakes to be (1.8 ± 0.9) and (2.8 ± 0.6) Pg a^{-1}, respectively, for the period 2012-2019. These values agree well with the corresponding CO_2 uptake values of (1.8 ± 1.1) (land) and (2.6 ± 0.5) Pg a^{-1} (ocean) reported by the GCP.

Additionally, our study has shown that our aircraft observation and the method we used to correct artificial fractionation of O_2 and N_2 are useful in evaluating inter-hemispheric air mixing processes based on the seasonal δ(APO) cycle, as well as interannual variations in the global air-sea O_2 flux, and in calculating global CO_2 budgets based on the long-term trends of $\delta_{cor.}(O_2/N_2)$ and CO_2 amount fraction.

Data availability.

The observational data of $\delta_{cor.}(O_2/N_2)$ and CO_2 amount fraction are available through the World Data Centre for Greenhouse Gases (WDCGG) at https://gaw.kishou.go.jp, and the respective DOIs are https://doi.org/10.50849/WDCGG_0006-8002-7001-05-02-9999 and https://doi.org/10.50849/WDCGG_0001-8002-1001-05-02-9999.

Author contributions.

SI designed the study, carried out measurements of $\delta(O_2/N_2)$, $\delta(Ar/N_2)$, $\delta(^{15}N)$, $\delta(^{18}O)$ and $\delta(^{40}Ar)$ and drafted the manuscript. KT, SK managed the collections, YN carried out the simulations of NICAM-TM using the supercomputer system (NEC SX-Aurora TSUBASA) of the National Institute for Environmental Studies (NIES). HM, SM and KI examined the results and provide feedback on the manuscript. All the authors approved the final manuscript.

Competing interests.

The authors declare that they have no conflict of interest.

Acknowledgements.

The authors gratefully acknowledge many staff members of the Japan Ministry of Defense and Japan Meteorological Agency for supporting the long-term observation.

Financial support.

This study was partly supported by the JSPS KAKENHI (grant nos. 15H02814 and 19H01975) and the Global Environment Research Coordination System from the Ministry of the Environment, Japan (grant nos. METI1454 and METI1953).

References

Andres, R. J., Boden, T., and Marland, G.: Monthly Fossil-Fuel CO_2 Emissions: Mass of Emissions Gridded by One Degree Latitude by One Degree Longitude, Carbon Dioxide Information Analysis Center, Oak Ridge National Laboratory, U.S. Department of Energy, Oak Ridge, Tenn., U.S.A., https://doi.org/10.3334/CDIAC/ffe.MonthlyMass.2016, 2016.

Aoki, N., Ishidoya, S., Matsumoto, N., Watanabe, T., Shimosaka, T., and Murayama, S.: Preparation of primary standard mixtures for atmospheric oxygen measurements with less than 1 μmol mol^{-1} uncertainty for oxygen molar fractions, Atmos. Meas. Tech., 12, 2631–2646, https://doi.org/10.5194/amt-12-2631-2019, 2019.

Aoki, N., Ishidoya, S., Tohjima, Y., Morimoto, S., Keeling, R. F., Cox, A., Takebayashi, S., and Murayama, S.: Intercomparison of O_2/N_2 ratio scales among AIST, NIES, TU, and SIO based on a round-robin exercise using gravimetric standard mixtures, Atmos. Meas. Tech., 14, 6181–6193, https://doi.org/10.5194/amt-14-6181-2021, 2021.

Bender, M. L., Ho, D. T., Hendricks, M. B., Mika, R., Battle, M. and co-authors.: Atmospheric O_2/N_2 changes, 1993-2002: Implications for the partitioning of fossil fuel CO_2 sequestration. Global Biogeochem. Cycles. 19, GB4017, doi:10.1029/2004GB002410, 2005.

Bent, J.: Airborne oxygen measurements over the Southern Ocean as an integrated constraint of seasonal biogeochemical processes, Ph.d. thesis, University of California, San Diego, 2014.

Birner, B., Chipperfield, M. P., Morgan, E. J., Stephens, B. B., Linz, M., Feng, W., Wilson, C., Bent, J. D., Wofsy, S. C., Severinghaus, J., and Keeling, R. F.: Gravitational separation of Ar/N_2 and age of air in the lowermost stratosphere in airborne observations and a chemical transport model, Atmos. Chem. Phys., 20, 12391– 12408, https://doi.org/10.5194/acp-20-12391-2020, 2020.

Bopp, L., Le Quéré, C., Heimann, M., Manning, A. C., and Mon- fray, P.: Climate-induced oceanic oxygen fluxes: implications for the contemporary carbon budget, Global Biogeochem. Cy., 16, 1022, https://doi.org/10.1029/2001GB001445, 2002.

Blaine, T. W.: Continuous measurements of atmospheric argon/ nitrogen as a tracer of air-sea heat flux: Models, methods, and data. Ph.D. thesis, Univ. of Calif., San Diego, La Jolla, 2005.

Eddebbar, Y. A., Long, M. C., Resplandy, L., Rödenbeck, C., Rodgers, K. B., Manizza, M., and Keeling, R. F.: Im- pacts of ENSO on air-sea oxygen exchange: Observations and mechanisms, Global Biogeochem. Cy., 31, 901–921, https://doi.org/10.1002/2017GB005630, 2017.

Garcia, H., and Keeling, R.: On the global oxygen anomaly and air-sea flux, J. Geophys. Res. 106 (C12), 31155-31166, 2001.

Gilfillan, D., Marland, G., Boden, T., and Andres, R.: Global, Regional, and National Fossil-Fuel CO_2 Emissions, Carbon Dioxide Information Analysis Center at Appalachian State University, Boone North Carolina, available at: https://energy.appstate.edu/CDIAC, 2019

Friedlingstein, P., O'Sullivan, M., Jones, M. W., Andrew, R. M., Hauck, J., Olsen, A., Peters, G. P., Peters, W., Pongratz, J., Sitch, S., Le Quéré, C., Canadell, J. G., Ciais, P., Jackson, R. B., Alin, S., Aragão, L. E. O. C., Arneth, A., Arora, V., Bates, N. R., Becker, M., Benoit-Cattin, A., Bittig, H. C., Bopp, L., Bultan, S., Chandra, N., Chevallier, F., Chini, L. P., Evans, W., Florentie, L., Forster, P. M., Gasser, T., Gehlen, M., Gilfillan, D., Gkritzalis, T., Gregor, L., Gruber, N., Harris, I., Hartung, K., Haverd, V., Houghton, R. A., Ilyina, T., Jain, A. K., Joetzjer, E., Kadono, K., Kato, E., Kitidis, V., Korsbakken, J. I., Landschützer, P., Lefèvre, N., Lenton, A., Lienert, S., Liu, Z., Lombardozzi, D., Marland, G., Metzl, N., Munro, D. R., Nabel, J. E. M. S., Nakaoka, S.-I., Niwa, Y., O'Brien, K., Ono, T., Palmer, P. I., Pierrot, D., Poulter, B., Resplandy, L., Robertson, E., Rödenbeck, C., Schwinger, J., Séférian, R., Skjelvan, I., Smith, A. J. P., Sutton, A. J., Tanhua,

T., Tans, P. P., Tian, H., Tilbrook, B., van der Werf, G., Vuichard, N., Walker, A. P., Wanninkhof, R., Watson, A. J., Willis, D., Wiltshire, A. J., Yuan, W., Yue, X., and Zaehle, S.: Global Carbon Budget 2020, Earth Syst. Sci. Data, 12, 3269–3340, https://doi.org/10.5194/essd-12-3269-2020, 2020.

Goto, D., Morimoto, S., Ishidoya, S., Aoki, S. and Nakazawa, T.: Terrestrial biospheric and oceanic CO_2 uptake estimated from long-term measurements of atmospheric CO_2 mole fraction, $\delta^{13}C$ and $\delta(O_2/N_2)$ at Ny-Ålesund, Svalbard. *J. Geophys. Res. Biogeosci.*, **122**, doi:10.1002/2017JG003845, 2017.

Gruber, N., Gloor, M., Fan, S.-M., and Sarmiento, J.: Air-sea flux of oxygen estimated from bulk data: Implications for the marine and atmospheric oxygen cycles, Global Biogeochem. Cy., 15, 783– 803, 2001.

Ishidoya, S., Morimoto, S., Sugawara, S., Watai, T., Machida, T. Aoki, S., Nakazawa, T., and Yamanouchi, T.: Gravitational separation suggested by O_2/N_2, $\delta^{15}N$ of N_2, $\delta^{18}O$ of O_2, Ar/N_2 observed in the lowermost part of the stratosphere at northern middle and high latitudes in the early spring of 2002, Geophys. Res. Lett., 35, L03812, doi:10.1029/2007GL031526, 2008.

Ishidoya, S., Aoki, S., Goto, D., Nakazawa, T., Taguchi, S., and Patra, P. K.: Time and space variations of the O_2/N_2 ratio in the troposphere over Japan and estimation of global CO_2 budget, Tellus B. 64, 18964, http://dx.doi.org/10.3402/tellusb.v64i0.18964, 2012.

Ishidoya, S., Sugawara, S., Morimoto, S., Aoki, S., Nakazawa, T., Honda, H., and Murayama, S.: Gravitational separation in the stratosphere – a new indicator of atmospheric circulation, Atmos. Chem. Phys. 13, 8787–8796, 2013, www.atmos-chem-phys.net/13/8787/2013/, doi:10.5194/acp-13-8787-2013, 2013.

Ishidoya, S., and Murayama, S.: Development of high precision continuous measuring system of the atmospheric O_2/N_2 and Ar/N_2 ratios and its application to the observation in Tsukuba, Japan, Tellus B, 66, 22574, http://dx.doi.org/10.3402/tellusb.v66.22574, 2014.

Ishidoya, S., Tsuboi, K., Matsueda, H., Murayama, S., Taguchi, S., Sawa, Y., Niwa, Y., Saito, K., Tsuji, K., Nishi, H., Y. Baba, Y., Takatsuji, S., Dehara, K., Fujiwara, H.: New atmospheric O_2/N_2 ratio measurements over the western North Pacific using a cargo aircraft C-130H, SOLA, 10, 23-28, doi:10.2151/sola.2014-006, 2014.

Ishidoya, S., Tsuboi, K., Murayama, S., Matsueda, H., Aoki, N., Shimosaka, T., Kondo, H., and Saito, K.: Development of a continuous measurement system for atmospheric O_2/N_2 ratio using a paramagnetic analyzer and its application in Minamitorishima Island, Japan, SOLA, 13, 230-234, 2017.

Ishidoya, S., Sugawara, S., Tohjima, Y., Goto, D., Ishijima, K., Niwa, Y., Aoki, N., and Murayama, S.: Secular change in atmospheric Ar/N_2 and its implications for ocean heat uptake and Brewer–Dobson circulation, Atmos. Chem. Phys., 21, 1357– 1373, https://doi.org/10.5194/acp-21-1357-2021, 2021.

IUPAC Green Book, 3rd edition, prepared for publication by E.R. Cohen, T. Cvitas, J.G Frey, B. Holmstrom, K. Kuchitsu, R. Marquardt, I. Mills, F. Pavese, M. Quack, J. Stohner, H. Strauss, M. Takami, and A.J. Thor, RSC Publishing, 2007.

Kawamura, K., Severinghaus, J., Ishidoya, S., Sugawara, S., Hashida, G., Motoyama, H., Fujii, Y., Aoki, S., and Nakazawa, T.: Convective mixing of air in firn at four polar sites, Earth and Planetary Science Letters, 244, 672-682., 2006.

Keeling, R. F.: Development of an interferometric oxygen analyzer for precise measurement of the atmospheric O_2 mole fraction, *Ph.D. thesis*, Harvard University, Cambridge, 1988.

Keeling, R. F. and Shertz, S. R. 1992. Seasonal and interannual variations in atmospheric oxygen and implications for the global carbon cycle, *Nature.* **358**, 723-727.

Keeling, R. F., Bender, M. L., and Tans, P. P.: What atmospheric oxygen measurements can tell us about the global carbon cycle, Global Biogeochem. Cycles, 7, 37-67, 1993.

Keeling, R. F., Stephens, B. B., Najjar, R. G., Doney, S. C., Archer, D., and Heimann, M.: Seasonal variations in the atmospheric O_2/N_2 ratio in relation to the kinetics of air-sea gas exchange. Global Biogeochem. Cycles. 12, 141-163, 1998.

Keeling, R. F., Blaine, T., Paplawsky, B., Katz, L., Atwood, C., and Brockwell, T.: Measurement of changes in atmospheric Ar/N_2 ratio using a rapid-switching, single-capillary mass spectrometer system, Tellus B: Chemical and Physical Meteorology, 56, 322–338, https://doi.org/10.3402/tellusb.v56i4.16453, 2004.

Keeling, R. F., Körtzinger, A., and Gruber, N.: Ocean deoxygenation in a warming world, Annu. Rev. Marin. Sci., 2, 199-229, doi:10.1146/annurev.marine.010908.163855, 2010.

Keeling, R. F. and Manning, A. C.: Studies of recent changes in atmospheric O_2 content, in Treatise on Geochemistry, vol. 5, 2nd ed., Elsevier, Amsterdam, 385–404, 2014.

Kobayashi, S., Ota, Y., Harada, Y., Ebita, A., Moriya, M., On- oda, H., Onogi, K., Kamahori, H., Kobayashi, C., Endo, H., Miyaoka, K., and Takahashi, K.: The JRA-55 Reanalysis: general specifications and basic characteristics, J. Meteorol. Soc. Jpn., 93, 5–48, https://doi.org/10.2151/jmsj.2015-001, 2015.

Le Quéré, C., Andrew, R. M., Friedlingstein, P., Sitch, S., Hauck, J., Pongratz, J., Pickers, P. A., Korsbakken, J. I., Peters, G. P., Canadell, J. G., Arneth, A., Arora, V. K., Barbero, L., Bastos, A., Bopp, L., Chevallier, F., Chini, L. P., Ciais, P., Doney, S. C., Gkritzalis, T., Goll, D. S., Harris, I., Haverd, V., Hoffman, F. M., Hoppema, M., Houghton, R. A., Hurtt, G., Ilyina, T., Jain, A. K., Johannessen, T., Jones, C. D., Kato, E., Keeling, R. F., Gold- ewijk, K. K., Landschützer, P., Lefèvre, N., Lienert, S., Liu, Z., Lombardozzi, D., Metzl, N., Munro, D. R., Nabel, J. E. M. S., Nakaoka, S.-I., Neill, C., Olsen, A., Ono, T., Patra, P., Peregon, A., Peters, W., Peylin, P., Pfeil, B., Pierrot, D., Poulter, B., Re- hder, G., Resplandy, L., Robertson, E., Rocher, M., Rödenbeck, C., Schuster, U., Schwinger, J., Séférian, R., Skjelvan, I., Stein- hoff, T., Sutton, A., Tans, P. P., Tian, H., Tilbrook, B., Tubiello, F. N., van der Laan-Luijkx, I. T., van der Werf, G. R., Viovy, N., Walker, A. P., Wiltshire, A. J., Wright, R., Zaehle, S., and Zheng, B.: Global Carbon Budget 2018, Earth Syst. Sci. Data, 10, 2141– 2194, https://doi.org/10.5194/essd-10-2141-2018, 2018.

Levitus, S., Antonov, J. I., Boyer, T. P., Baranova, O. K., Garcia, H. E., Locarnini, R. A., Mishonov, A. V., Reagan, J. R., Seidov, D., Yarosh, E. S., and Zweng, M. M.: World ocean heat content and thermosteric sea level change (0–2000 m), 1955–2010, Geophys. Res. Lett., 39, L10603, https://doi.org/10.1029/2012GL051106, 2012.

Manning, A. C. and Keeling, R. F.: Global oceanic and terrestrial biospheric carbon sinks from the Scripps atmospheric oxygen flask sampling network. Tellus B. 58, 95– 116, 2006.

McKinley, G. A., Follows, M. J, Marchall, J., and Fan, S.-M.: Inter- annual variability of air-sea O_2 fluxes and the determination of CO_2 sinks using atmospheric O_2/N_2, Geophys. Res. Lett., 30(3), 1101, doi:10.1029/2002GL016044 ,2003.

Morgan, E. J., Stephens, B. B., Long, M. C., Keeling, R. F., Bent, J. D., McKain, K., Sweeney, C., Hoecker- Martínez, M. S., and Kort, E. A.: Summertime Atmo- spheric Boundary Layer Gradients of O_2 and CO_2 over the Southern Ocean, J. Geophys. Res., 124, 13439–13456, https://doi.org/10.1029/2019JD031479, 2019.

Nakazawa, T., Ishizawa, M., Higuchi, K., and Trivett, N. B. A.: Two curve fitting methods applied to CO_2 flask data. Environmetrics. 8, 197-218, 1997a.

Nakazawa, T., Morimoto, S., Aoki, S. and Tanaka, M.: Temporal and spatial variations of the carbon isotopic ratio of atmospheric carbon dioxide in the western Pacific region, J. Geophys. Res., 102, 1271-1285, 1997b.

Nevison, C. D., Mahowald, N. M., Doney, S. C., Lima, I. D., and Cassar, N.: Impact of variable air-sea O_2 and CO_2 fluxes on atmospheric potential oxygen (APO) and land- ocean carbon sink partitioning, Biogeosciences, 5, 875–889,https://doi.org/10.5194/bg-5-875-2008, 2008.

Nevison, C. D., Keeling, R. F., Kahru, M., Manizza, M., Mitchell, B. G., Cassar N.: Estimating net community production in the Southern ocean based on atmospheric potential oxygen and satellite ocean color data, Glob. Biogeochem. Cycles., 26, GB1020. DOI: http://dx.doi.org/10.1029/2011GB004040, 2012.

Niwa, Y., Tomita, H., Satoh, M., and Imasu, R.: A Three-Dimensional Icosahedral Grid Advection Scheme Preserving Monotonicity and Consistency with Continuity for Atmospheric Tracer Transport, J. Meteorol. Soc. Jpn., 89, 255–268, doi:10.2151/jmsj.2011-306, 2011.

Niwa, Y., Machida, T., Sawa, Y., Matsueda, H., Schuck, T. J., Brenninkmeijer, C. A. M., Imasu, R., and Satoh, M.: Imposing strong constraints on tropical terrestrial CO2 fluxes using passenger aircraft based measurements, J. Geophys. Res., 117, doi:10.1029/2012JD017474, 2012.

Niwa, Y., Tsuboi, K., Matsueda, H., Sawa, Y., Machida, T., Nakamura, M., Kawasato, T., Saito, K., Takatsuji, S., Tsuji, K., Nishi, H., Dehara, K., Baba, Y., Kuboike, D., Iwatsubo, S., Ohmori, H., and Hanamiya, Y.: Seasonal Variations of CO_2, CH_4, N_2O and CO in the Mid-troposphere over the Western North Pacific Observed using a C-130H Cargo Aircraft, J. Meteorol. Soc. Japan, 92(1), doi:10.2151/jmsj.2014-104, 2014.

Rödenbeck, C., Le Quéré, C., Heimann, M., and Keeling, R. F.: Interannual variability inoceanic biogeochemical pro- cesses inferred by inversion of atmospheric O_2/N_2 and CO_2 data, Tellus B, 60, 685–705, https://doi.org/10.1111/j.1600-0889.2008.00375.x, 2008.

Satoh, M., Matsuno, T., Tomita, H., Miura, H., Nasuno, T., and Iga, S.: Nonhydrostatic icosahedral atmospheric model (NICAM) for global cloud resolving simulations, J. Comput. Phys., 227, 3486– 3514, doi:10.1016/j.jcp.2007.02.006, 2008.

Satoh, M., Tomita, H., Yashiro, H., Miura, H., Kodama, C., Seiki, T., Noda, A. T., Yamada, Y., Goto, D., Sawada, M., Miyoshi, T., Niwa, Y., Hara, M., Ohno, T., Iga, S., Arakawa, T., Inoue, T., and Kubokawa, H.: The Non-hydrostatic Icosahedral

Atmospheric Model: description and development, Progress in Earth and Planetary Science, 1, 1–32, doi:10.1186/s40645-014-0018-1, 2014.

Severinghaus, J.: Studies of the terrestrial O_2 and carbon cycles in sand dune gases and in biosphere 2, *Ph. D. thesis, Columbia University*, New York, 1995.

Steinbach, J.: Enhancing the usability of atmospheric oxygen measurements through emission source characterization and airborne measurement, Ph.D. thesis, Friedrich-Schiller-Universität, 2010.

Stephens, B. B., Keeling, R. F., Heimann, M., Six, K., Murnane, R. and co-authors.: Testing global ocean carbon cycle models using measurements of atmospheric O_2 and CO_2 concentration. *Global Biogeochem. Cycles* **12** (2), 213-230, 1998.

Stephens, B. B., Keeling, R. F. and Paplawsky, W. J. 2003. Shipboard measurements of atmospheric oxygen using a vacuum-ultraviolet absorption technique. *Tellus B.* **55**, 857–878.

Stephens, B. B., Morgan, E. J., Bent, J. D., Keeling, R. F., Watt, A. S., Shertz, S. R., and Daube, B. C.: Airborne measurements of oxygen concentration from the surface to the lower stratosphere and pole to pole, Atmos. Meas. Tech., 14, 2543–2574, https://doi.org/10.5194/amt-14-2543-2021, 2021.

Sturm, P., Leuenberger, M., Moncrieff, J. and Ramonet, M. 2005. Atmospheric O_2, CO_2 and $\delta^{13}C$ measurements from aircraft sampling over Griffin Forest, Perthshire, UK. *Rapid Commun. Mass Spectrom.* **19**, 2399-2406, doi:10.1002/rcm.2071.

Takahashi, T., Sutherland, S. C., Wanninkhof, R., Sweeney, C., Feely, R. A., Chipman, D. W., Hales, B., Friederich, G., Chavez, F., Sabine, C., Watson, A., Bakker, D. C. E., Schuster, U., Metzl, N., Yoshikawa-Inoue, H., Ishii, M., Midorikawa, T., Nojiri, Y., Körtzinger, A., Steinhoff, T., Hoppema, M., Olafsson, J., Arnar- son, T. S., Tilbrook, B., Johannessen, T., Olsen, A., Bellerby, R., Wong, C. S., Delille, B., Bates, N. R., and de Baar H. J. W.: Cli- matological mean and decadal change in surface ocean pCO_2, and net sea-air CO_2 flux over the global oceans, Deep Sea Res. Pt. II, 56, 554–577, https://doi.org/10.1016/j.dsr2.2008.12.009, 2009.

Tohjima, Y., Machida, T., Watai, T., Akama, I., Amari, T., and Moriwaki, Y.: Preparation of gravimetric standards for measurements of atmospheric oxygen and reevaluation of atmospheric oxygen concentration, J. Geophys. Res., 110, D1130, 2005.

Tohjima, Y., Mukai, H., Nojiri, Y., Yamagishi, H. and Machida, T.: Atmospheric O_2/N_2 measurements at two Japanese sites: estimation of global oceanic and land biotic carbon sinks and analysis of the variations in atmospheric potential oxygen (APO). *Tellus B.* **60**, 213-225, 2008.

Tohjima, Y., Minejima, C., Mukai, H., Machida, T., Yamag- ishi, H., and Nojiri, Y.: Analysis of seasonality and annual mean distribution of atmospheric potential oxygen (APO) in the Pacific region, Glob. Biogeochem. Cy., 26, GB4008, https://doi.org/10.1029/2011GB004110, 2012.

Tohjima, Y., Mukai, H., Machida, T., Hoshina, Y., and Nakaoka, S.-I.: Global carbon budgets estimated from atmospheric O_2/N_2 and CO_2 observations in the western Pacific region over a 15-year period, Atmos. Chem. Phys., 19, 9269–9285, https://doi.org/10.5194/acp-19-9269-2019, 2019.

Trenberth, K. E.: Seasonal variations in global sea level pressure and the total mass of the atmosphere, J. Geophys. Res., 86, 5238– 5246, 1981.

Tsuboi, K., Matsueda, H., Sawa, Y., Niwa, Y., Nakamura, M., Kuboike, D., K. Saito, K., Ohmori, H., Iwatsubo, S., Nishi, H., Hanamiya, Y., Tsuji, K., and Baba, Y.: Evaluation of a new JMA aircraft flask sampling system and laboratory trace gas analysis system, Atoms. Meas. Tech., 6, 1257−1270, doi: 10.5194/amt-6-1257-2013, 2013.

Van der Laan, S., van der Laan-Luijk, I.T., Rödenbeck, C., Varlagin, A., Shironya, I. and Neubert, R.E.M, Ramonet, M.: Atmospheric CO_2, $\delta(O_2/N_2)$, APO and oxidative ratios from aircraft flask samples over Fyodorovskoye, Western Russia, Atmos. Environ., 97, 174-181, 2014.

Weiss, R. F.: The solubility of nitrogen, oxygen and argon in water and seawater, Deep-Sea Res., 17, 721–735, 1970.

Wofsy et al.: HIAPER Pole-to-Pole Observations (HIPPO): fine grained, global-scale measurements of climatically important atmospheric gases and aerosols, Philos. T. Roy. Soc. A, 369, 2073– 2086, https://doi.org/10.1098/rsta.2010.0313, 2011.

Zhao, C. L. and Tans, P. P.: Estimating uncertainty of the WMO mole fraction scale for carbon dioxide in air, J. Geophys. Res., 111, D08S09, doi:10.1029/2005JD006003, 2006.

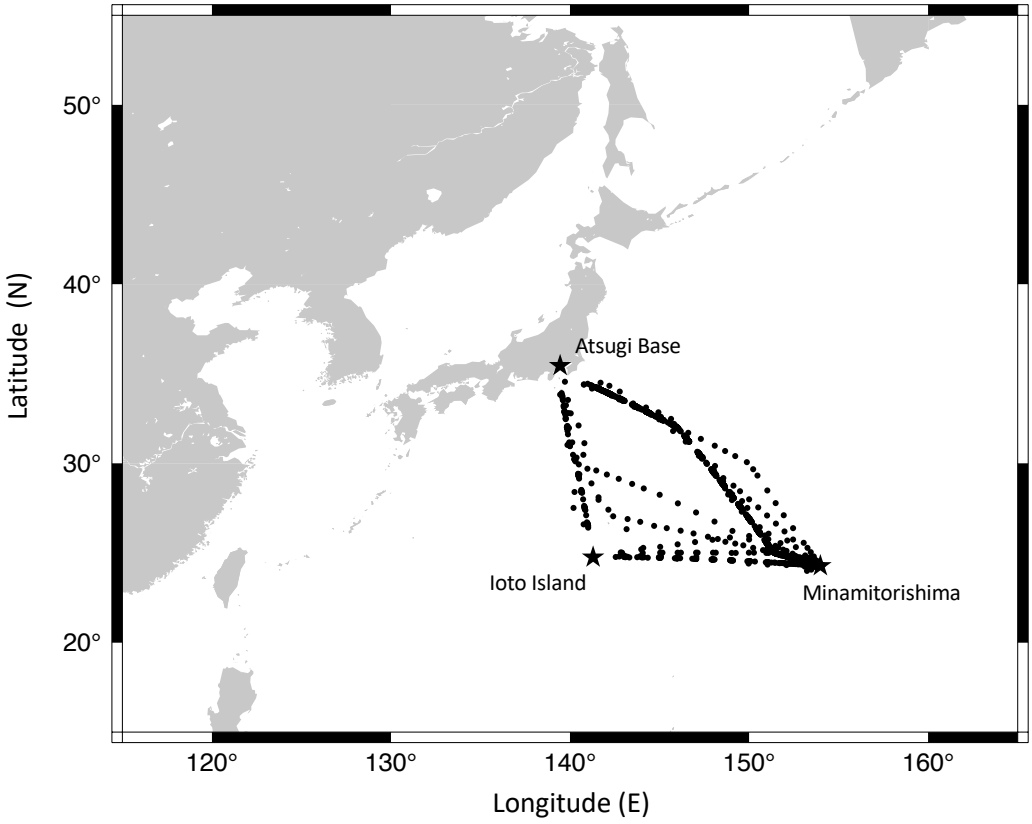

625

Figure 1: Locations of C-130 aircraft air sampling for the period May 2012 – March 2020 (circles). Locations of Minamitorishima (MNM), Ioto Island, and Atsugi Base are also shown by stars. Latitudinal and vertical distributions are taken during the level flight and descent portion at MNM, respectively. 2,206 of air samples were collected in total, and 1,783 of them were analyzed for O_2/N_2 and Ar/N_2 ratios, as well as the stable isotopic ratios of N_2, O_2 and Ar.

630

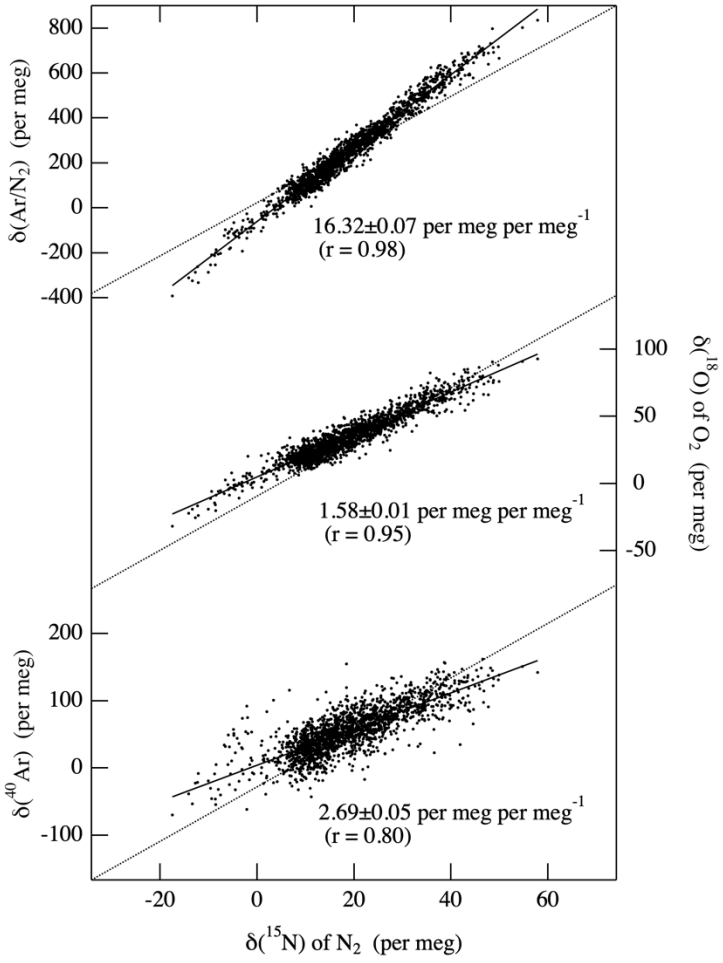

635 **Figure 2: Measured $\delta(Ar/N_2)$, $\delta(^{18}O)$ of O_2 and $\delta(^{40}Ar)$ plotted against $\delta(^{15}N)$ of N_2 for all the collected air samples (solid dots). Least-squares regression lines fitted to the data are shown as solid lines, while the relationships expected from mass-dependent fractionation of air molecules are shown by dotted lines.**

640

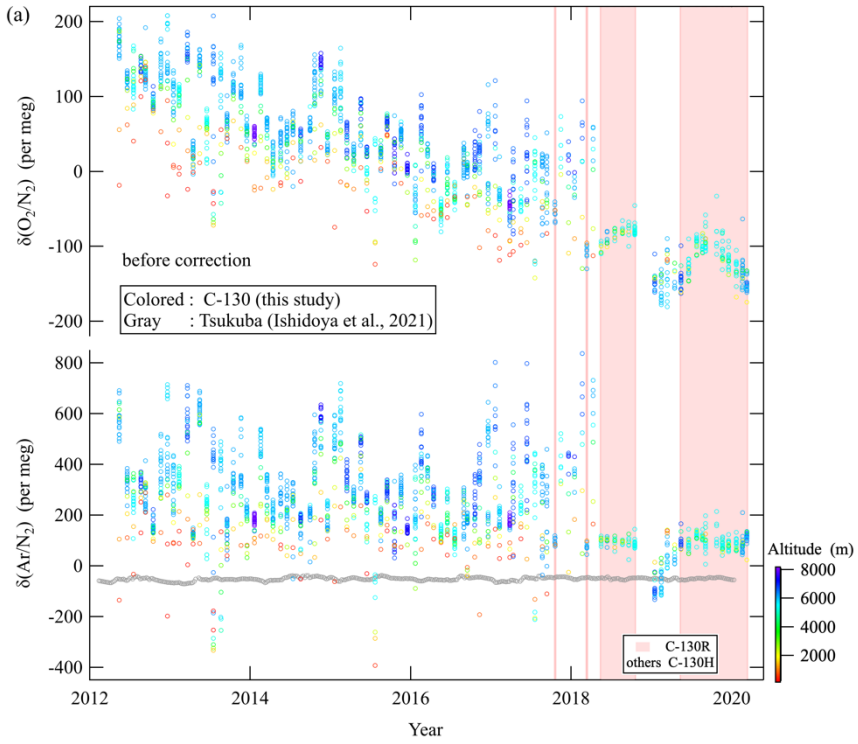
(a)
δ(O2/N2) (per meg)
before correction
Colored : C-130 (this study)
Gray : Tsukuba (Ishidoya et al., 2021)
δ(Ar/N2) (per meg)
C-130R
others C-130H
Altitude (m)
8000
6000
4000
2000
Year

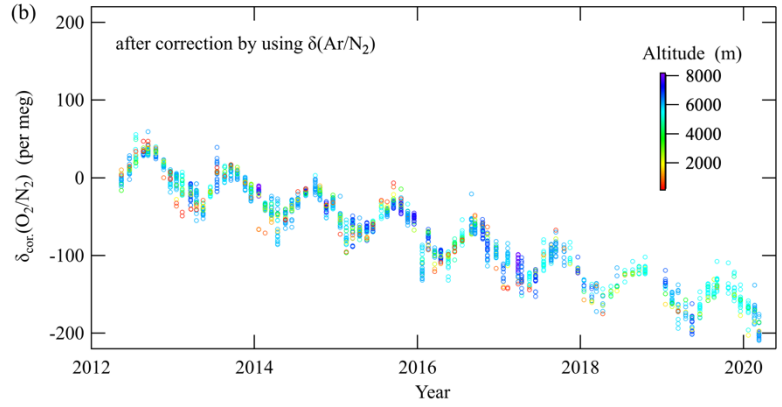
(b)
after correction by using δ(Ar/N2)
δcor.(O2/N2) (per meg)
Altitude (m)
8000
6000
4000
2000
Year

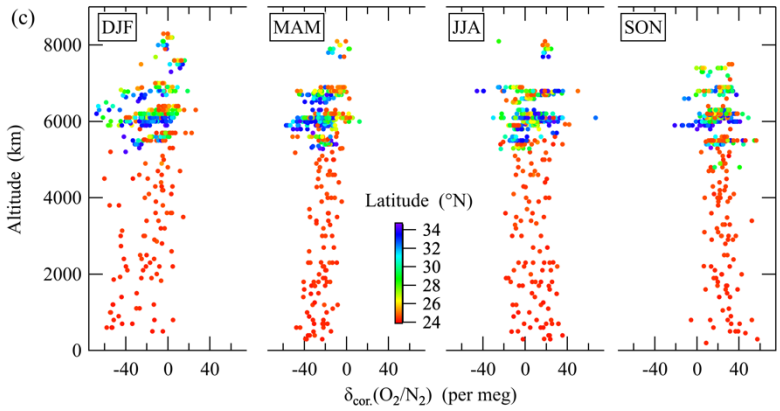

Figure 3: (a) Measured values of $\delta(O_2/N_2)$ and $\delta(Ar/N_2)$ for all the air samples collected onboard the C-130 aircraft. $\delta(Ar/N_2)$ values observed at Tsukuba, Japan are also shown as gray circles (Ishidoya et al., 2021). Shaded areas denote the periods when C-130R aircraft was used, and C-130H aircraft was used in other periods. Color bar indicates the altitude where the air sampling were carried out. (b) $\delta_{cor.}(O_2/N_2)$ corrected for artificial fractionation by applying eq. (6) (see text). Color bar indicates the altitude where the air sampling were carried out. (c) Vertical profiles of detrended $\delta_{cor.}(O_2/N_2)$ separated by season (DJF: December to February, MAM: March to May, JJA: June to August, and SON: September to November), obtained by subtracting a linear secular trend, fitted to the $\delta_{cor.}(O_2/N_2)$ in (b), from each $\delta_{cor.}(O_2/N_2)$ value. Color bar indicates the latitude where the air sampling were carried out.

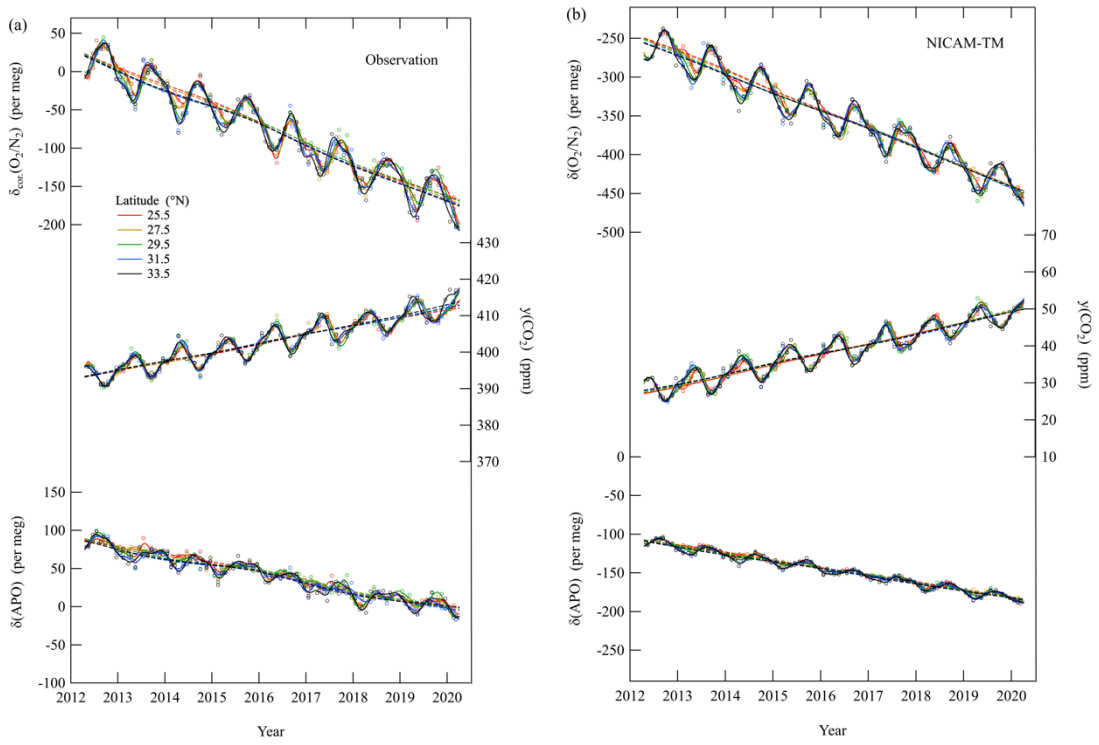

Figure 4: (a) $\delta_{cor.}(O_2/N_2)$, CO_2 amount fraction and δ(APO) observed at the height of (6.1 ± 0.5) (±1σ) km at various latitudes over the western North Pacific. Best-fit curves to the data (solid lines) and secular trends (dashed lines) are also shown. (b) Same as in (a) but for calculated values obtained from the NICAM-TM control-run. The data from NICAM-TM are reported on arbitrary scales different from those of observations.

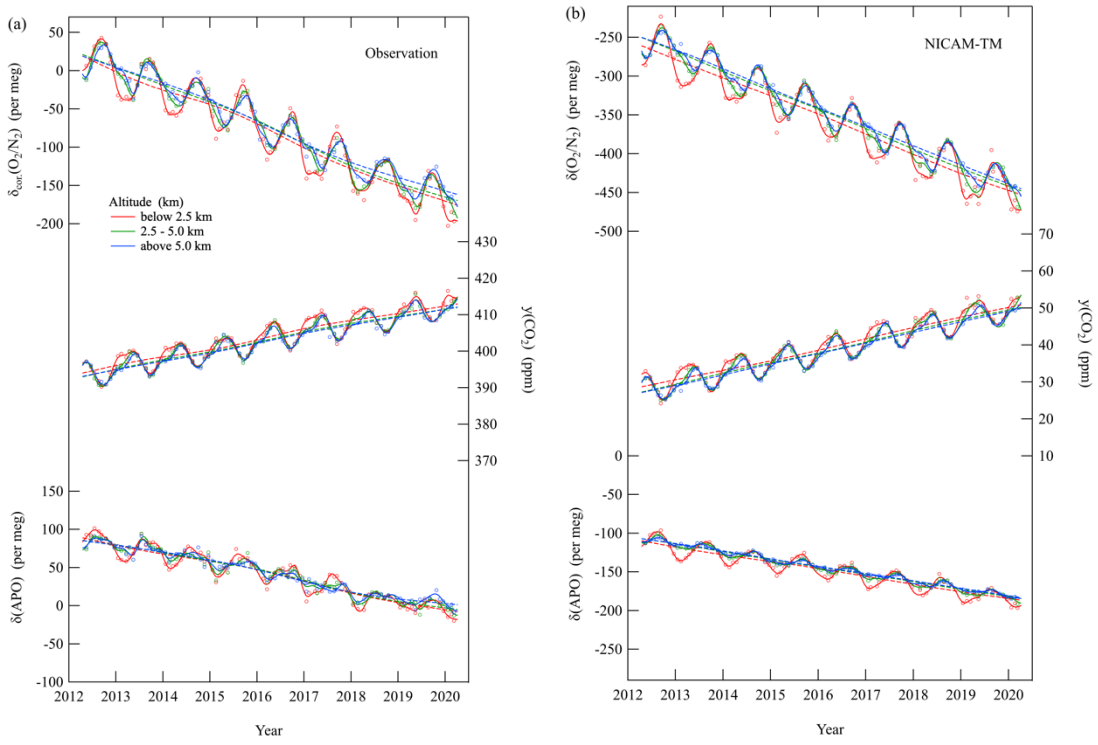

665 **Figure 5: (a) $\delta_{cor.}(O_2/N_2)$., CO_2 amount fraction and δ(APO) observed in the troposphere over MNM at various altitudes. Best-fit curves to the data (solid lines) and secular trends (dashed lines) are also shown. (b) Same as in (a) but for calculated values using NICAM-TM. The data from NICAM-TM are reported on arbitrary scales different from those of observations.**

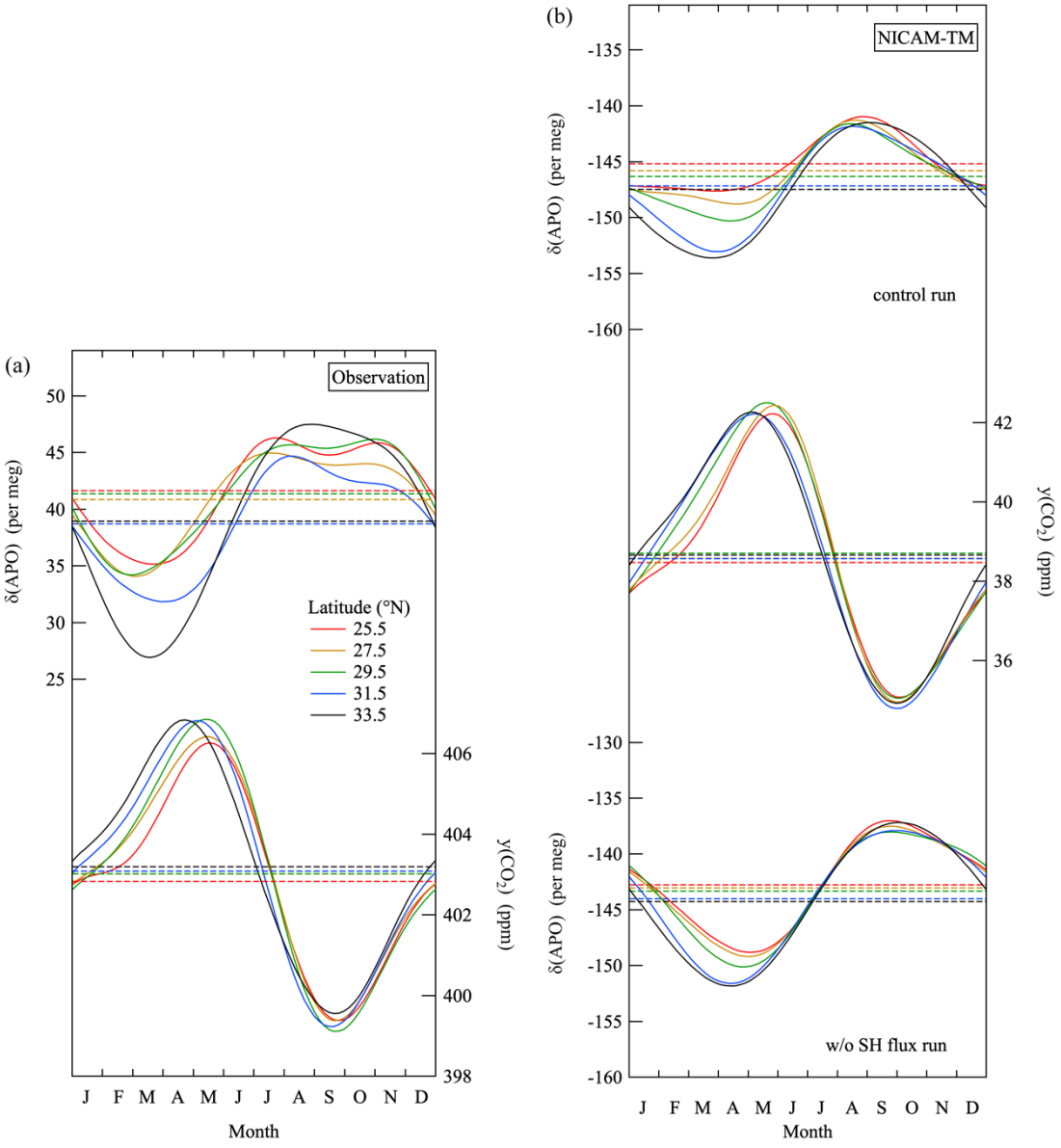
(a)
Observation
δ(APO) (per meg)
γ(CO2) (ppm)
Latitude (°N)
25.5
27.5
29.5
31.5
33.5
J F M A M J J A S O N D
Month
(b)
NICAM-TM
control run
w/o SH flux run
δ(APO) (per meg)
γ(CO2) (ppm)
J F M A M J J A S O N D
Month

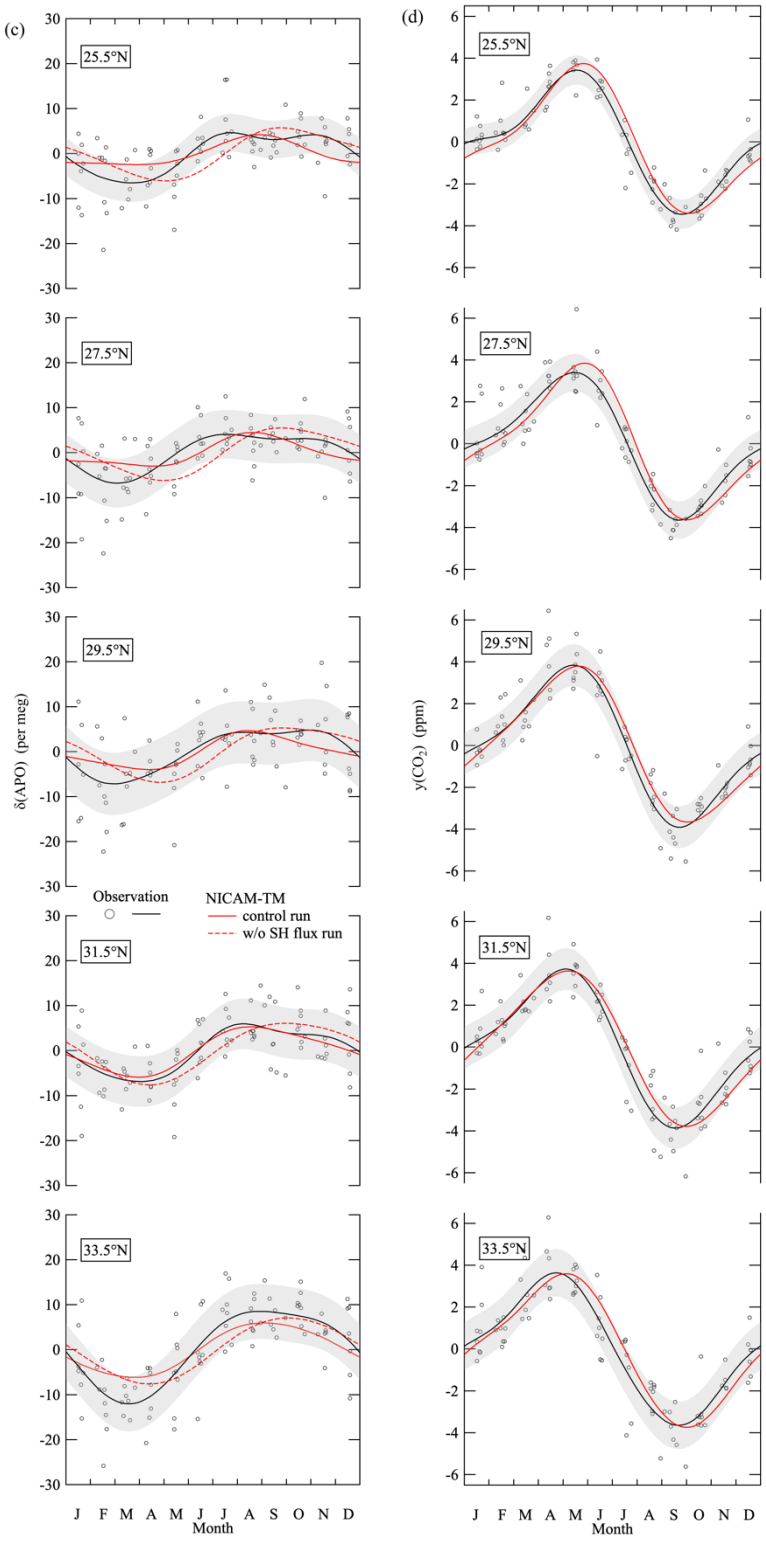
(c)
(d)
25.5°N
27.5°N
29.5°N
31.5°N
33.5°N
δ(APO) (per meg)
y(CO2) (ppm)
Observation
NICAM-TM
control run
w/o SH flux run
J F M A M J J A S O N D
Month

Figure 6: (a) Average seasonal cycles of δ(APO) and CO_2 amount fraction observed in the troposphere at various latitudes over the western North Pacific. Dashed lines denote the average values throughout the observation period. (b) Same as in (a) but for calculated values obtained from the NICAM-TM control run and the corresponding results from the w/o SH flux run (see text). (c) Same average seasonal cycles of the observed and simulated δ(APO) in (a) and (b) along with the detrended observed values at each latitude. Error bands (shaded) indicate standard deviations of the observed δ(APO) from the average seasonal cycles ($\pm 1\sigma$). (d) Same as in (c) but for CO_2 amount fraction.

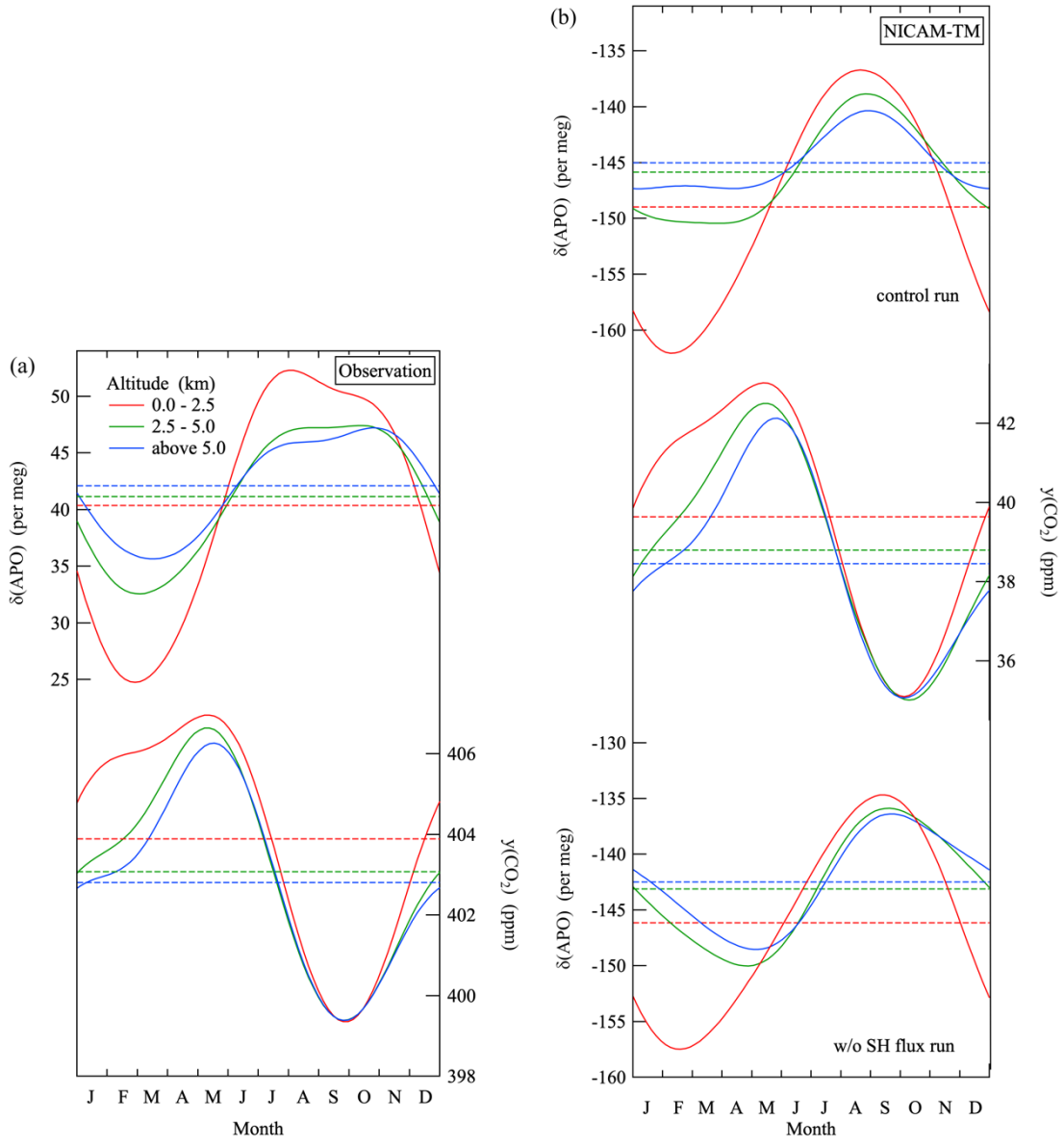
(a)
Observation
Altitude (km)
0.0 - 2.5
2.5 - 5.0
above 5.0
δ(APO) (per meg)
y(CO2) (ppm)
J F M A M J J A S O N D
Month
(b)
NICAM-TM
control run
w/o SH flux run
δ(APO) (per meg)
y(CO2) (ppm)
J F M A M J J A S O N D
Month

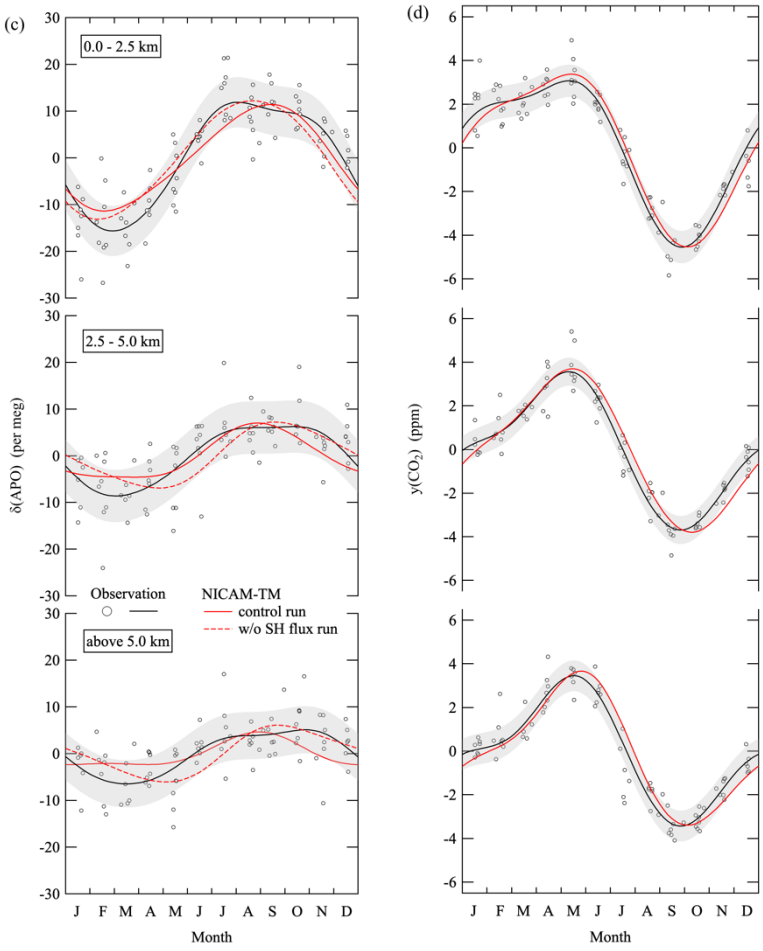

Figure 7: Same as in Fig. 6 but for those in the troposphere over MNM.

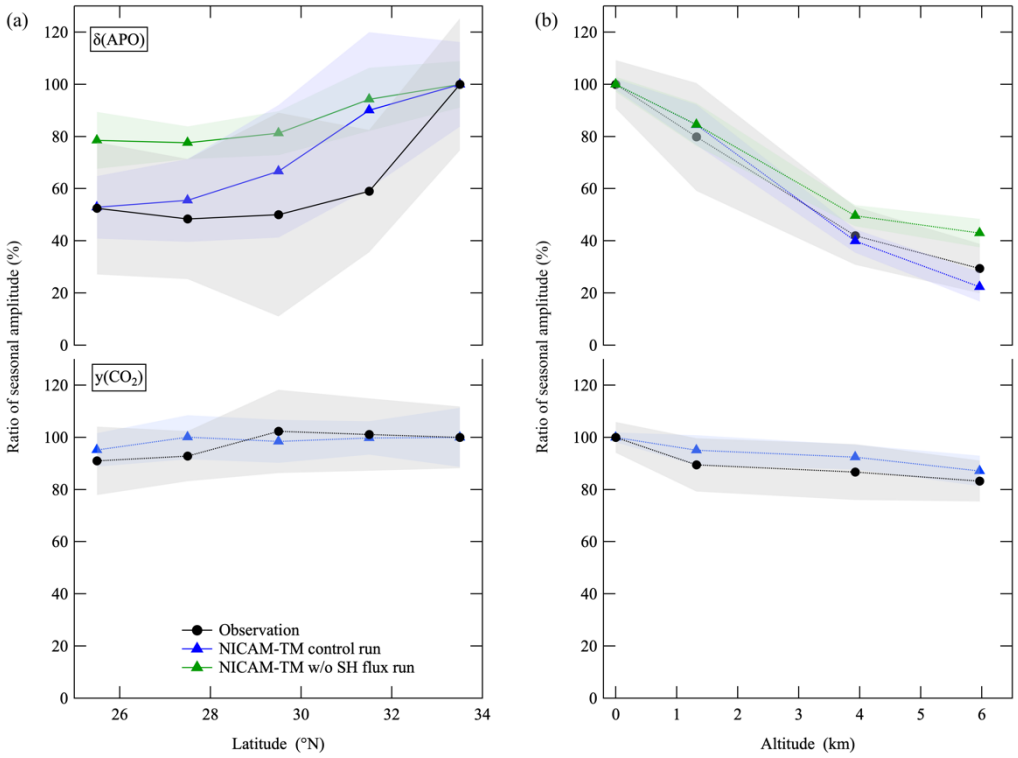

Figure 8: (a) Latitudinal distribution of average ratios of the observed seasonal δ(APO) and CO_2 amount fraction amplitudes calculated relative to the values observed at 33.5° N in the troposphere over the western North Pacific throughout the observation period (black filled circles). Error bands (shaded) indicate year-to-year variations (±1σ). The corresponding results calculated using NICAM-TM control run (blue triangles) and w/o SH flux run (green triangles) are also shown. Amplitude of seasonal APO cycle was calculated as a difference between an average value during July to September and that during February to April considering its broad peak, while that of CO_2 amount fraction was evaluated as a difference between a seasonal maximum and minimum values. (b) Same as in (a) but for vertical distribution over MNM relative to the corresponding surface values, and amplitude of seasonal APO cycle was evaluated as a difference between an average value during July to October and that during February to April.

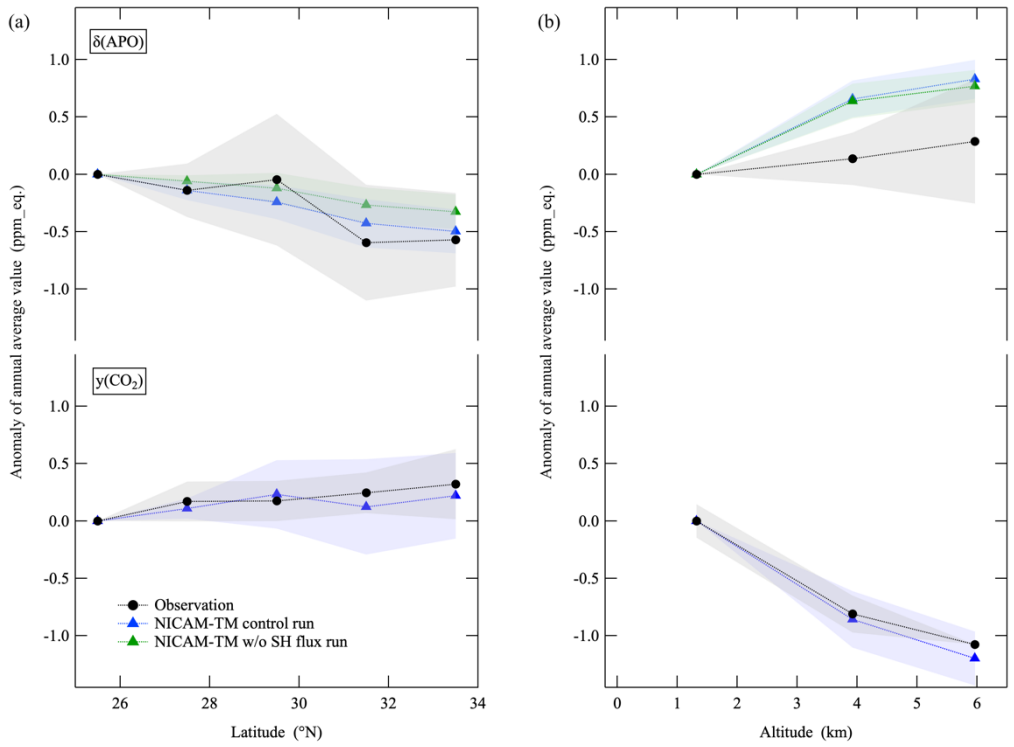

Figure 9: (a) Latitudinal distribution of average deviations of the annual mean values of δ(APO) and CO_2 amount fraction relative to those at 25.5° N in the troposphere over the western North Pacific throughout the observation period (black filled circles). Error bands (shaded) indicate year-to-year variations (±1σ). The corresponding results calculated using NICAM-TM for control run (blue triangles) and w/o SH flux run (green triangles) are also shown. (b) Same as in (a) but for vertical distribution over MNM relative to the corresponding values at 1.3 km.

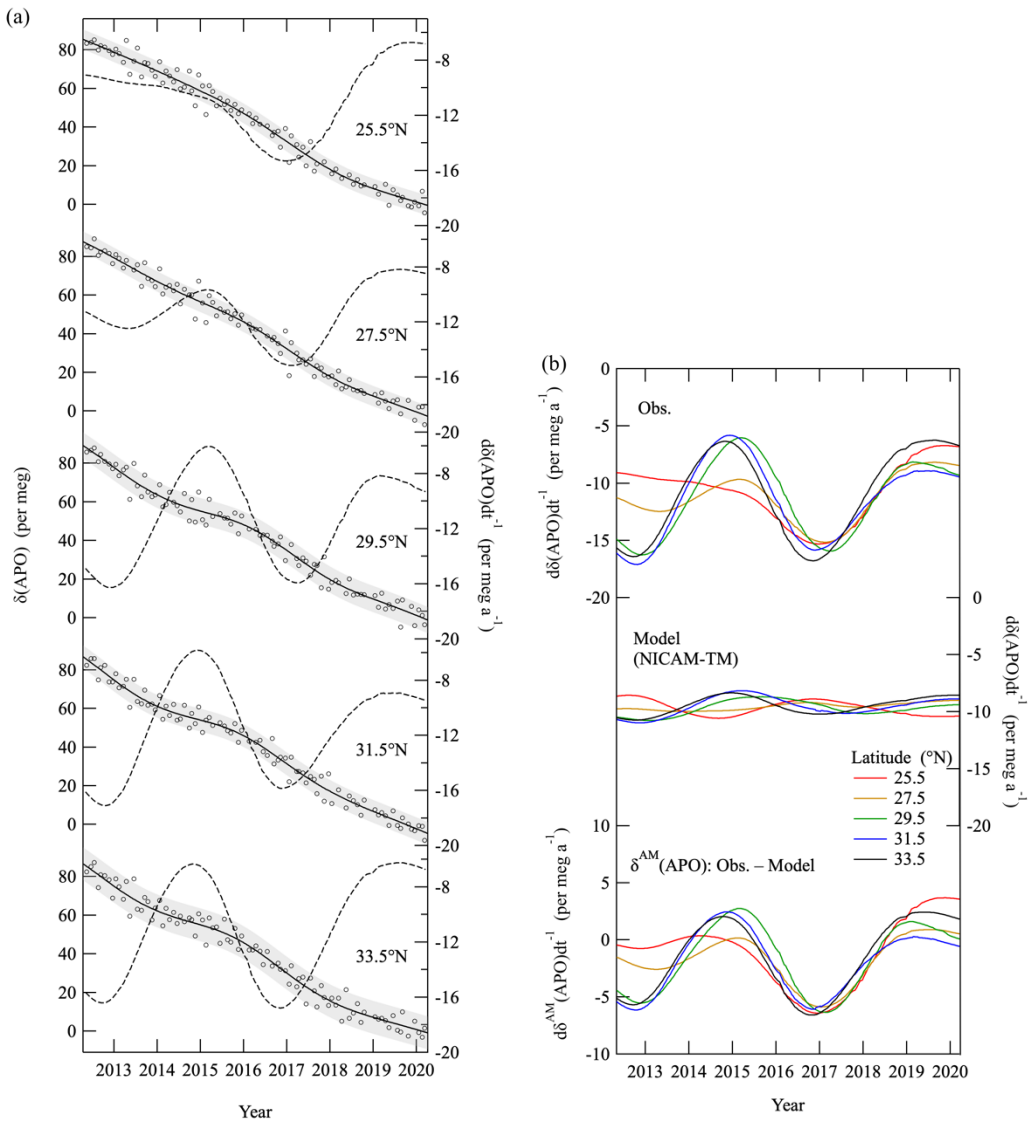

Figure 10: (a) Same secular trends in Fig. 4(a) and their annual change rates along with the deseasonalised values of δ(APO) at each latitude over the western North Pacific. Error bands (shaded) indicate standard deviations of the deseasonalised δ(APO) from the secular trends (±1σ). (b) Same annual change rates in (a) (top). The corresponding change rates for the APO obtained from the control run of NICAM-TM (middle) and those of δ^{AM}(APO) obtained by subtracting the calculated δ(APO) from the observed δ(APO) (bottom) are also shown.

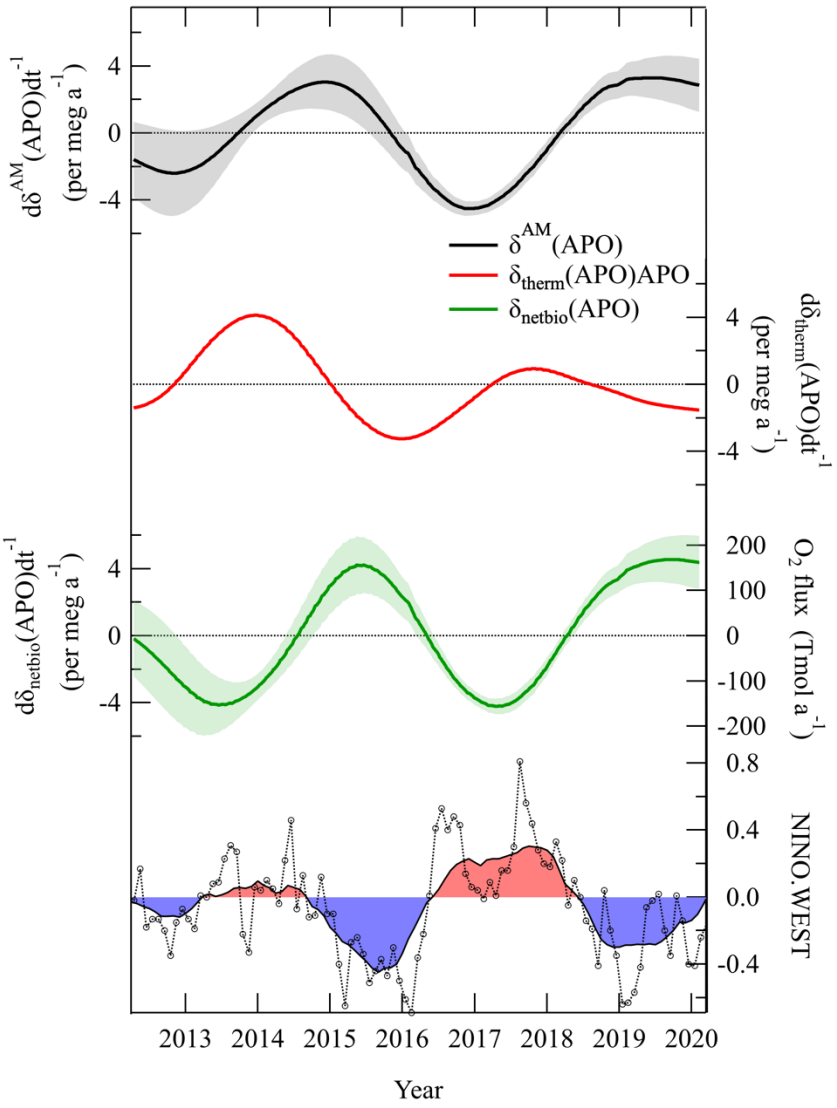

725

Figure 11: Anomaly in the average annual change rate of δ^{AM}(APO) shown at the bottom of Fig. 10 (thick black line). Anomaly in the change rate of APO driven only by the solubility change, expected from the observed surface δ(Ar/N_2) at Tsukuba, Japan (δ_{therm}(APO); red line, see text), and that driven by the net marine biospheric activities (δ_{netbio}(APO); green line) obtained by subtracting the change rate of δ_{therm}(APO) from that of δ^{AM}(APO) are shown. Anomaly in the global air-sea O_2 flux corresponding
730 **to the change rate of δ_{netbio}(APO) is also shown (see text). The time series of the NINO.WEST index (black open circles) and the annual average values of the index (thin black line) are shown at the bottom of the figure.**